FINAL SCIENTIFIC/TECHNICAL REPORT

1. COVER PAGE DATA ELEMENTS:

Report Title: Compact Ceramic Microchannel Heat Exchangers
Type of Report: Final Scientific/Technical Report
Reporting Period Start Date: October 1, 2017
Reporting Period End Date: September 30, 2016
Principal Author: Dr. Charles A. Lewinsohn
Date Report was Issued: February 17, 2017
DOE Award Number: DE-FE0024077
Name and Address of Submitting Organization: Ceramatec, Inc., 2425 South 900 West, Salt Lake City, UT 84119
Name and Address of Significant Subcontractor: Colorado School of Mines, 1500 Illinois Street, Golden, CO 80401

ACKNOWLEDGEMENT: This material is based upon work supported by the Department of Energy under Award Number DE-FE0024077.

2. ACCOMPLISHMENTS:

a. Major goals

The major goals of the project are:

(1) Design tools will be verified and validated by the fabrication and testing of both heat exchanger plates and heat exchanger stacks consisting of multiple heat exchanger plates joined together.
(2) Fabrication methods will be demonstrated and performed using commercial-scale equipment that allows for initial estimates of manufacturing costs.
(3) Preliminary approaches to integration with the balance of plant of power generation systems will be demonstrated.
(4) Prototype performance data, of critical importance in developing this technology will be obtained under controlled conditions, to demonstrate the benefits of compact, ceramic microchannel heat exchanger systems.

An update of the status of the project milestones is given below:

Table 1

Milestone Name	SOPO Task	Planned Completion Date	Status
Design Requirements Specification Sheet	2.1	End Q1	COMPLETE
Initial Heat Exchanger Plate Design	2.3	End Q1	COMPLETE
Heat Exchanger Plate Design for Stack Fabrication and Testing	3.3	End Q4	COMPLETE
Assembly of Prototype Heat Exchanger Stack	4.0	End Q6	COMPLETE
Completion of Prototype Stack Testing	5.0	End Q8	COMPLETE

b. Accomplishments

In summary, by performing the tasks described in the initial proposal, all of the milestones were met. The objective of the proposed work was to demonstrate the feasibility of a step change in power plant efficiency at a commercially viable cost, by obtaining performance data for prototype, compact, ceramic microchannel heat exchangers. This will advance the technology from Technology Readiness Level 3 (TRL 3) to Technology Readiness Level 4 (TRL 4) and validate the potential of using these heat exchangers for enabling high efficiency solid oxide fuel cell (SOFC) or high-temperature turbine-based power plants. The following report will describe how this objective was met.

In collaboration with The Colorado School of Mines (CSM), specifications were developed for a high temperature heat exchanger for three commercial microturbines. Microturbines were selected because are a more mature commercial technology than SOFC, they are a low-volume and high-value target for market entry of high-temperature heat exchangers, and they are essentially scaled-down versions of turbines used in utility-scale power plants. Using these specifications, microchannel dimensions were selected to meet the performance requirements. Ceramic plates were fabricated with microchannels of these dimensions. The plates were tested at room temperature and elevated temperature. Plates were joined together to make modular,

heat exchanger stacks that were tested at a variety of temperatures and flow rates. Although gas flow rates equivalent to those in microturbines could not be achieved in the laboratory environment, the results showed expected efficiencies, robust operation under significant temperature gradients at high temperature, and the ability to cycle the stacks. Details of the methods and results are presented below.

Task 1.0 – Project Management and Planning

This task included all work elements required to maintain and revise the Project Management Plan and to manage and report on activities in accordance with the plan. It included the necessary activities to ensure coordination and planning of the project with DOE/NETL and other project participants. This included the submission and approval of required NEPA documentation. A revised version of the Project Management Plan was provided to the appropriate DOE staff at the beginning of the project.

Task 2.0 – Heat Exchanger Plate Design and Analysis

This task involved utilizing numerical models, previous results and data, and publically reported literature to design a ceramic, microchannel plate as the basic repeat unit for the heat exchanger stacks fabricated in Task 4 and tested in Task 5. The task was divided into the following subtasks.

Subtask 2.1 Definition of Design Requirements

In collaboration with Dr. Robert Kee and Dr. Robert Braun, at CSM, design requirements for heat exchange for commercial, gas-fired microturbines were determined. Dr. Braun used information publically disclosed by Capstone Turbine Corporation to determine the temperature, pressures and flow rates at various state points within a microturbine system, indicated in Figure 1.

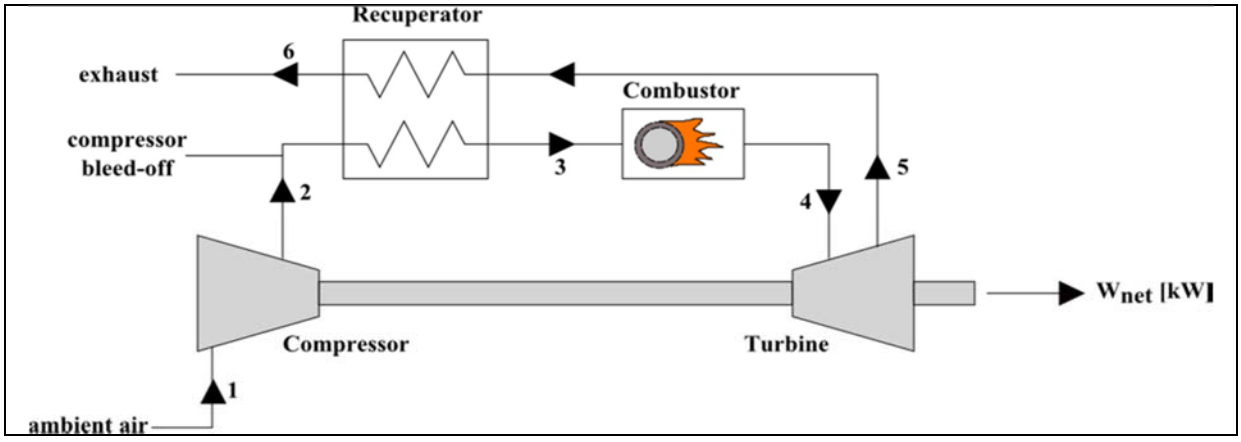

Figure 1 Schematic of simple microturbine system used for determining heat exchanger specifications.

Thermodynamic models of system components were used in conjunction with properties of appropriate mixtures of air and natural gas. The turbine inlet temperature and compression ratio were obtained from literature. Fitting parameters were adjusted so that the model predicted performance and conditions reported in Capstone's product brochure. Results are show in Table 2. This analysis provided the requirements for heat exchanger (recuperator) gas flow rates, pressure drop, temperatures, heat transfer and effectiveness, shown in Table 3. These requirements became the design parameters for the microchannel heat exchanger components, as described below.

Table 2

Turbine		C30	C65	C200
Turbine Inlet Temp	(C)	900	938	950
Compression Ratio		3.2	3.67	4.3
Recuperator Pressure Drop	(kPa)	10	7.5	7.5
Combustor Pressure Drop	(kPa)	25	25	25
Recuperator Pinch Temperature	(C)	105	119	72
Reported System Efficiency	(%)	26	29	33
Calculated System Efficiency	(%)	26.41	29	33.89
Reported Exhaust Flow	(kg/s)	0.31	0.49	1.3
Calculated Exhaust Flow	(kg/s)	0.3015	0.5027	1.36
Reported Exhaust Temperature	(C)	275	309	280
Calculated Exhaust Temperature	(C)	275.3	309.3	280.7
Recuperator Heat Transfer	(kW)	140.9	215.2	585.8
Recuperator Effectiveness		0.799	0.763	0.843
Air-Fuel Ratio		124.7	105.3	108.2

Table 3

Turbine Model and Net Power	(kW)	C30	C65	C200
Pressure Drop	(kPa)	10	7.5	7.5
Air Side Mass Flow Rate	(kg/s)	0.2991	0.498	1.348
Exhaust Side Mass Flow Rate	(kg/s)	0.3051	0.5027	1.36
Air Inlet Temp (State Point 2)	(C)	149.4	168.1	190.6
Air Outlet Temp (State Point 3)	(C)	589.4	571.6	594.7
Exhaust Inlet Temp (State Point 5)	(C)	694.4	690.6	666.7
Exhaust Outlet Temp (State Point 6)	(C)	275.3	309.3	280.7
Recuperator Heat Transfer	(kW)	140.9	215.2	585.8
Recuperator Effectiveness		0.799	0.7632	0.8427

Subtask 2.2 – Thermal / Flow Design

The Colorado School of Mines, under the direction of Dr. R.J. Kee, performed computational fluid dynamics (CFD) modeling, using FLUENT software, of single microchannels to establish optimum channel dimensions for the specifications determined in Subtask 2.1. Channel widths were varied from 0.6-2.0 mm. The channel height was varied from 0.4-0.8 mm. The thickness of the channel side wall was set to 0.4 mm. The thickness of the floor and ceiling of the channel was varied from 0.4-1.0 mm. Channels were assumed to be 150 mm long (the full length of a heat exchanger plate). The mass flow rate through the channel was calculated for Reynolds' numbers of 400, 600, and 800, since laminar flow reduces pressure drop. The mass flow rate external to the channel was set by the ratio of mass flow rates calculated in the system model. Using this method, the size of the heat exchanger would vary according to the Reynolds' number since more channels would be required to support the total mass flow rate as the Reynolds' number decreased. A single channel, however, represents the behavior of any channel in the heat exchanger, regardless of the overall system size. Due to the inherent modularity of the design of

the components and stacks, all of the results obtained are relevant to a heat exchanger system of any size, i.e. thermal duty, that uses the same channel and/or plate dimensions.

CFD analysis was performed using elements 0.5 mm-long in the flow direction and 0.05 mm-long in the other two directions. Mesh refinement studies were performed to verify that the results were independent of the mesh size. The pressure drop as a function of channel width was calculated for a range of channel heights and Reynolds number. The results are shown in Figure 2. The lines are not calculated, but are included to help differentiate the results for different combinations of channel height and Reynolds number. The results show that, as expected, low Reynolds number and larger channel heights lead to lower pressure drop. Low Reynolds number, however, implies low mass flow rates and larger heat exchanger size. Furthermore, for channels larger than 1.2 mm-wide, the width of the channel doesn't affect the pressure drop.

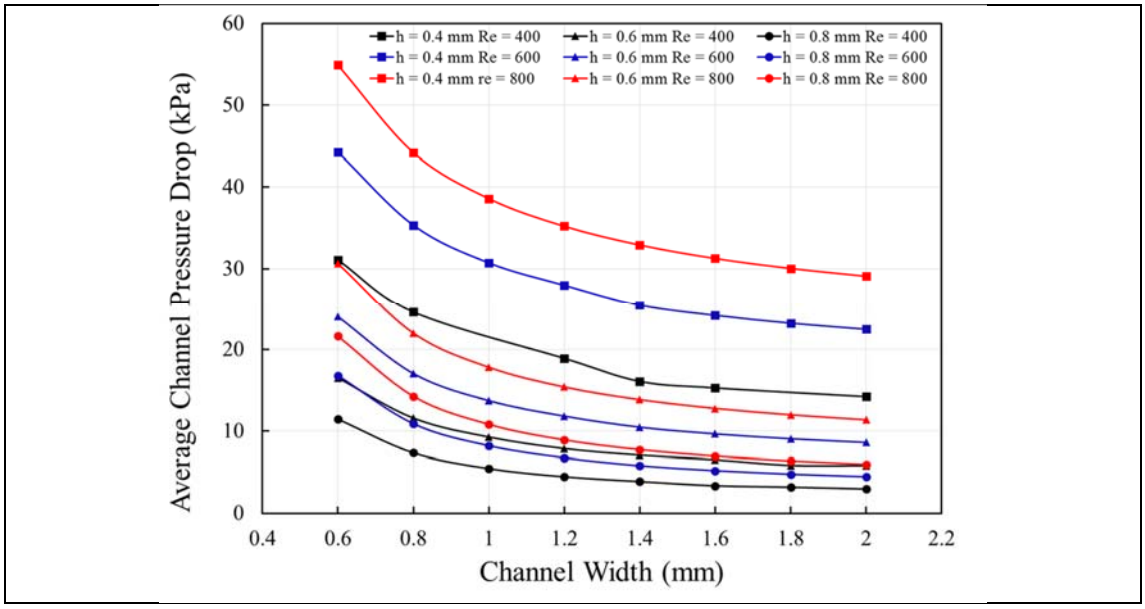

Figure 2 Channel pressure drop vs. width for a range of Reynolds number and channel heights.

The effect of hydraulic on channel pressure drop was also modeled. As the height of the channel increased, the allowable Reynolds number and hydraulic diameter increased. The results, shown in Figure 3, show that hydraulic diameters larger than 0.60 mm are preferable for low pressure drop (<20 kPa).

The effect of channel width, channel height and Reynolds number on effectiveness was also modeled. The results, shown in Figure 4, also show that effectiveness doesn't vary with channel width for channels wider than 1.2 mm. The effectiveness, however, increases as the Reynolds number decreases and the channel height decreases, counter to the trends for pressure drop. Therefore, a channel height of 0.6 mm, a width of 0.8 mm, and a Reynolds number of 600 were selected to obtain effectiveness >80% and pressure drop < 20 kPa. These values were used by Ceramatec to accomplish the second Technical Milestone of Task 2: the initial design for the heat exchanger plate discussed in Section 3, especially section 3.1.2 of this report.

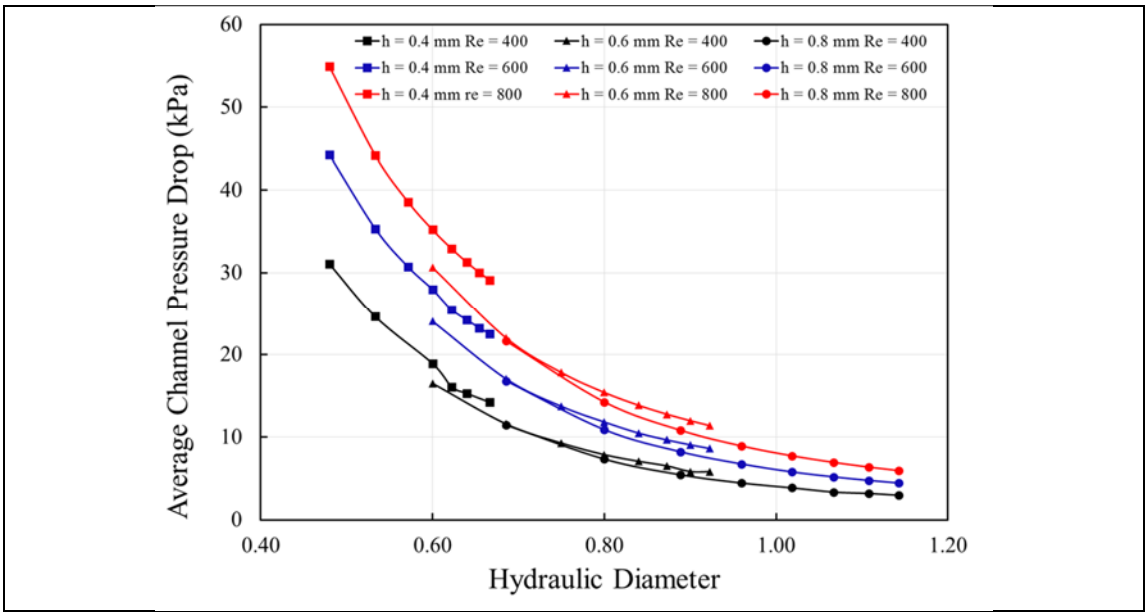

Figure 3 Channel pressure drop as a function of channel hydraulic diameter and various combinations of channel height and Reynolds number.

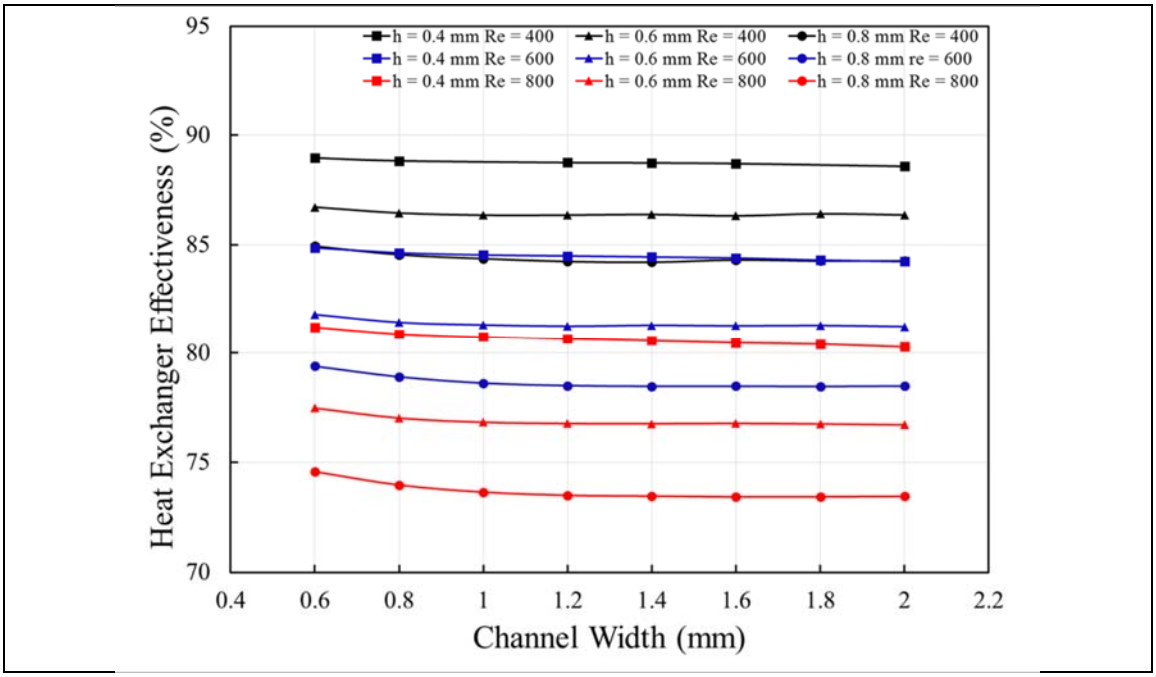

Figure 4 Effect of channel width on heat exchanger effectiveness.

Subtask 2.3 – Thermo-Mechanical Design

In this task mechanical design issues are considered through modeling efforts. Designing heat exchangers with high reliability requires knowledge of the mechanical stress induced by thermal loads, fluid pressures and mechanical interfaces. The design procedure is multi-faceted, where manufacturing, material, thermal and structural inputs are required. This mechanical modeling effort may require the thermal profiles generated from the conjugate mass and heat

transfer models of Task 2.2. When results are compared to experimental data, the heat exchanger plates can be optimized to the design criteria. Outputs from Subtasks 2.2 and 2.3 may require iterative design and modelling to satisfy competing design requirements or for optimization. This subtask was performed by The Colorado School of Mines, under the guidance of Dr. R.J. Kee who provided the following sub-sections (2.3.1-2.3.4), co-authored by his graduate assistant, Ms. Gandhali Kogekar (with minor formatting changes).

2.3.1 Model Geometry and Properties

Microchannel heat exchangers typically have channel dimensions of the order of millimeters or less. Fabrication of such demands careful attention to flow and structural characteristics. Thus, predicting flow profiles in heat exchanger prototypes before actually manufacturing, becomes very important and cost saving. Usually computational fluid dynamics (CFD) tools are used to simulate flow and energy profiles on different geometries of these heat exchangers to obtain an optimized design. To resolve temperature and heat flux profiles, a fine and conformal mesh is required near fluid-solid boundary interaction. Typically, for these micro channel heat exchangers, the mesh count goes beyond millions of mesh cells and it takes quite a long time to run these simulations. In this report, the thermal performance of a micro channel heat exchanger is studied by performing CFD simulations on a large mesh (more than 0.8 million cells) on multiple nodes.

In this project, a micro channel counter-flow heat exchanger with ten cold and ten hot fluid channels has been modeled and simulated using ANSYS software. The schematic of a micro channel heat exchanger is shown in Figure 20. The flow, being three dimensional and complicated, is solved using ANSYS Fluent. The dimensions and operating conditions for simulation are given in Table 4 and Table 5 respectively.

To study the effects of solid wall material on heat exchanger effectiveness and thermal stress, three materials with different conductivities are studied. The default material configuration considered here is alumina and air as solid and fluid materials, respectively. The second configuration is same as the first one, only the thermal conductivity is reduced to a very low value in order to see the temperature effects on the flow profiles. The third configuration uses silicon carbide (SiC) as the solid material. Table 6 shows properties of all the materials.

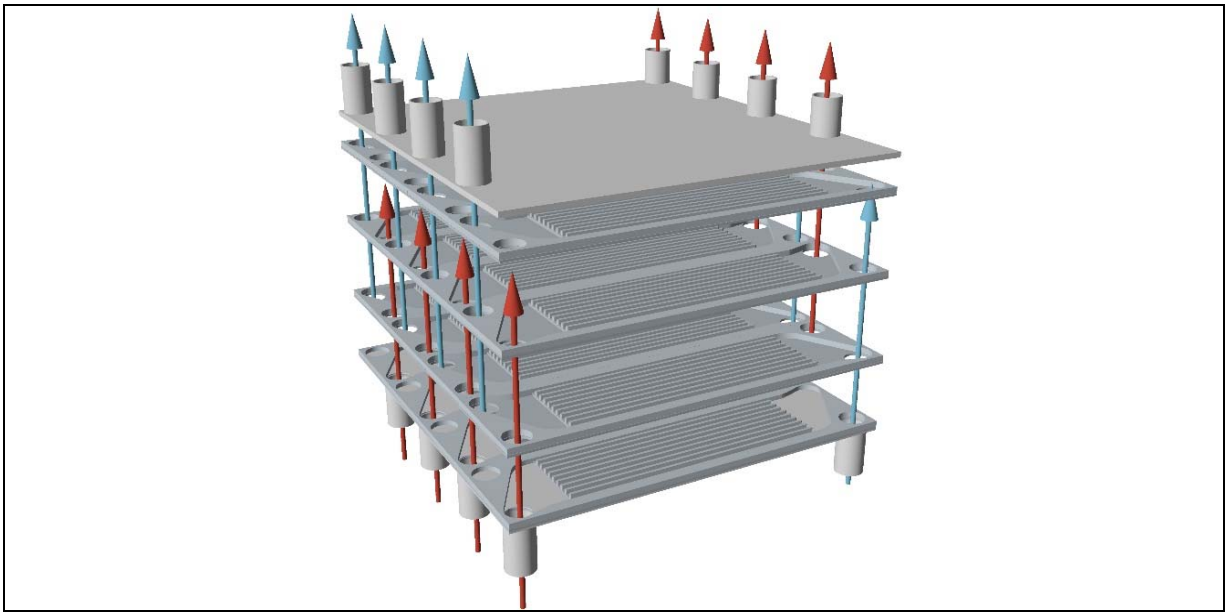

Figure 5 Microchannel heat exchanger geometry

Table 4
Channel Properties

Channel property	**Value**
Major length (a)	2 mm
Minor length (b)	1 mm
Aspect ratio (ε)	0.5
Cross sectional area of channels (A_c)	2 mm^2
Channel length (L)	0.1 cm
Number of channels	10
Thickness of the solid wall (t)	1 mm
Hydraulic diameter of channel(D_h)	1.33 mm

Table 5
Boundary conditions

Property	Boundary location	Value
Mass flow rate	Cold fluid inlet	0.001 kg/s
	Hot fluid inlet	0.001 kg/s
Temperature	Cold fluid inlet	300 K
	Hot fluid inlet	900 K
Pressure	Cold fluid inlet	0 Pa
	Hot fluid inlet	0 Pa

Table 6
Material properties

Property	Configuration		
	1	2	3
Density (kg m^3)	3750	3750	3100
Specific heat (J/kg K)	880	880	750
Conductivity (W/mK)	35	2	120
Young's modulus (GPa)	413	413	410
Poisson's ratio	0.33	0.33	0.14

2.3.2 Effectiveness calculations for microchannel heat exchanger

A steady-state solution for fluid flow and temperature profiles is obtained using ANSYS Fluent. Figure 6 shows temperature contours for cold as well as hot fluid planes. The effectiveness of the heat exchanger is calculated as:

$$\varepsilon = \frac{\mathrm{C_h}(T_{h,i} - T_{h,o})}{\mathrm{C_{min}}(T_{h,i} - T_{c,i})}$$

Or

$$\varepsilon = \frac{\mathrm{C_c}(T_{c,o} - T_{c,i})}{\mathrm{C_{min}}(T_{h,i} - T_{c,i})}$$

Where, the capacity rates are defined as

$$C = \dot{m} C_p$$

The inlet temperatures for cold and hot fluid are 300 K and 900 K respectively. The current model assumes constant heat capacity values for both the hot and cold fluids. The heat-exchanger effectiveness can be evaluated using either the cold or the hot fluid as

$$\varepsilon_h = \frac{(900 - T_{h,o})}{600}$$

Or

$$\varepsilon = \frac{(T_{c,o} - 300)}{600}$$

The effectiveness and outlet temperatures for three configurations are given in Table 7. As the thermal conductivity is increased, the effectiveness is reduced. The highest effectiveness is obtained for configuration 2 (Alumina with very low thermal conductivity). From this result, the role of axial conduction in the microchannel, counter-flow heat exchangers is evident.

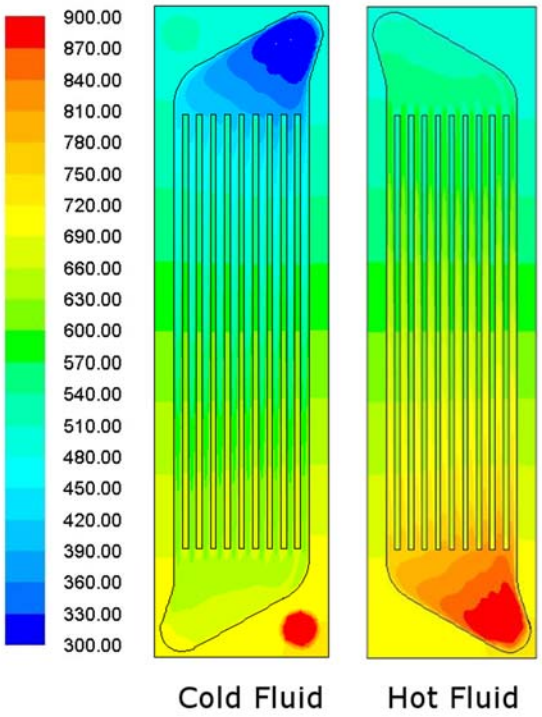

Figure 6 Temperature profiles for cold and hot fluid

Table 7
Effectiveness of heat exchanger

	Configuration		
	1	2	3
Hot outlet temperature (K)	519	483	558
Cold outlet temperature (K)	677	718	633
Effectiveness (ε_h)	0.635	0.695	0.570
Effectiveness (ε_c)	0.628	0.697	0.555

2.3.23 Thermal Stress Analysis of Steady State Solution

After getting a converged steady state solution, the next step is to check if this heat exchanger can sustain thermal stresses induced inside. The steady state temperature is imported to ANSYS Structural (with one way FSI) and thermal stresses are calculated as shown in Figure 7. The typical value for maximum sustainable stress for alumina is about 100 MPa. As seen from Figure 7, thermal stresses in the entire domain do not exceed 100 MPa and thus this geometry can sustain the thermal load. There are some locations where this stress magnitude is higher (up to 1 GPa), but these high stresses are artifacts generated due to sharp corners in the geometry. Because of manufacturing limitations, no real heat exchanger has such sharp corners, and thus such high stresses will not be generated in real cases. [Ceramatec comment: *Ideal structures typically have sharp corners that generate singularities in numerical model solutions. Our standard way to evaluate geometrical features that can appear as singularities in numerical models is to introduce radii and refine the mesh at these features to more closely approximate the actual elastic stress field. We often apply a shell layer with artificial properties to obtain more*

realistic results. Finally, we extensively validate all model predictions and designs using experimental testing.]

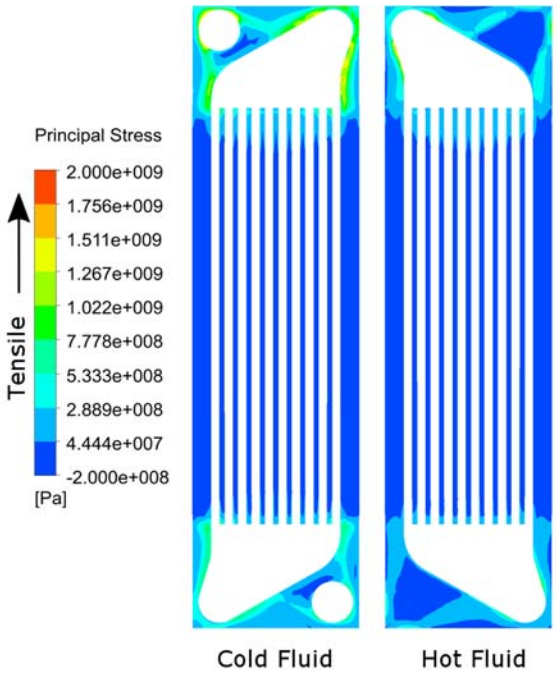

Figure 7 Thermal stresses on cold and hot fluid planes

Additionally, the maximum deformation for this heat exchanger is of the order of microns as shown in Figure 8. The channel dimensions are in millimeters and thus deformation of the order of microns is acceptable. This maximum deformation is observed near the sharp corners of the heat exchanger geometry (which again is impossible in practice).

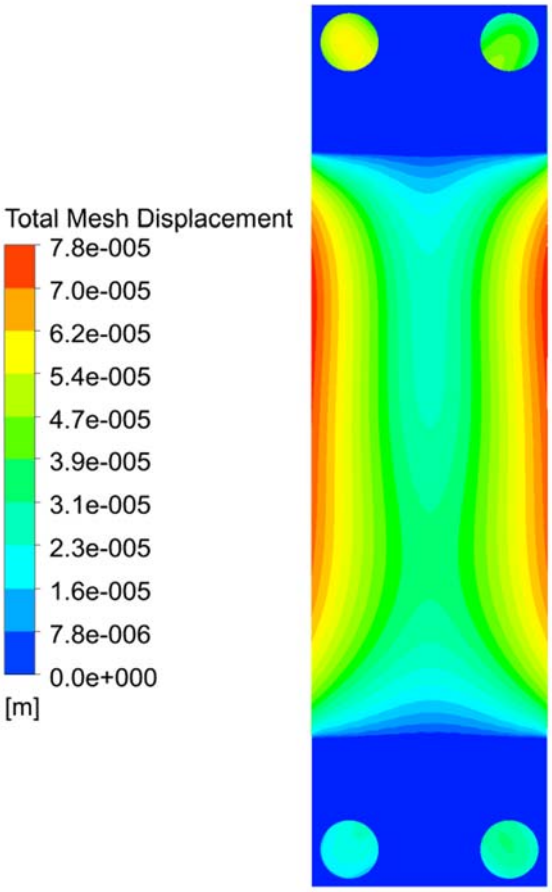

Figure 8 Deformation for full CFD model

2.3.4 Summary and Conclusions

A three dimensional, microchannel, counter flow heat exchanger has been evaluated using ANSYS. The effect of different thermal conductivity materials on heat exchanger effectiveness is analyzed. Additionally, thermal stresses generated inside the heat exchanger were studied using ANSYS Structural. The deformation and thermal stresses were found to be within acceptable sustainable limits.

Task 3.0 – Heat Exchanger Plate Fabrication & Testing

Subtask 3.1 Heat Exchanger Plate Fabrication

Successful fabrication of silicon carbide SiC HX plates requires several steps starting from silicon carbide powder and ultimately yielding a functional SiC microchannel HX plate and stack (module) that functions in heat exchange applications. The various processing steps include the following: SiC tape batching and casting, laser featuring of tape layers to introduce microchannels, lamination of appropriately featured layers to make an individual plate, densification of plates by thermally de-binding and sintering, joining of several plates together to make heat exchanger stacks, and attachment of manifolds for connection with the rest of the system.

As part of Ceramatec's roadmap to commercialization of ceramic, microchannel heat exchangers, processes were developed on commercial scale equipment in a pilot scale

manufacturing environment. To facilitate manufacturing scale-up and continuous process improvement via six-sigma style, lean manufacturing approaches, a database enabling traceability of materials and process parameters at each processing step from initial batching to final stack assembly was developed. Furthermore, database analysis is essential for both improving process yield and reducing cost of stacks and also for understanding the relationships among performance and testing results and fabrication methods. This database was developed using Microsoft Access, with Figure 9 showing a screen shot capture of various processing stages that are fully traceable.

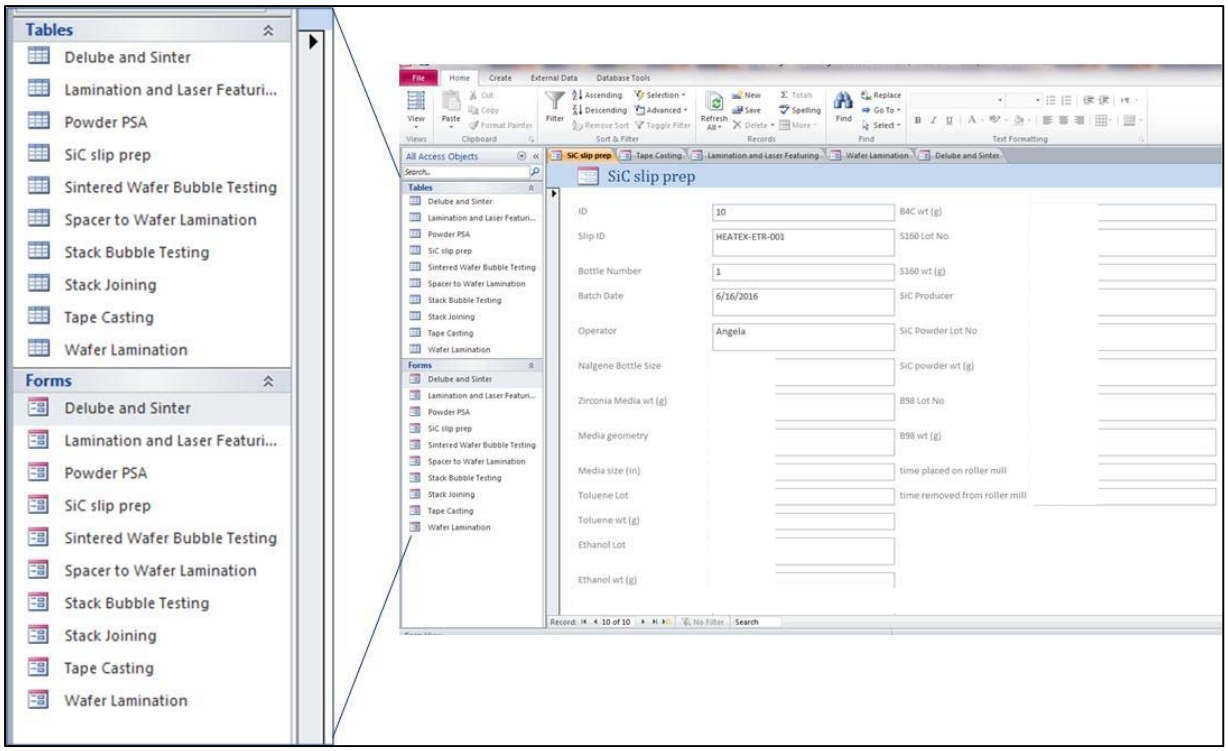

Figure 9 SiC HX processing data base (screen shot capture), created using Microsoft access, allowing full traceability of various process levels traversed in the creation of HX plates and stacks. The left side shows a ballooned section of the captured image revealing more clearly the various process levels that are recorded.

3.1.1 SiC tape batching and casting

Using a methodology for formulating and developing tapes from new powder source, refined using industrial cost-share funds, a formulation and process conditions for casting tapes containing SiC powder that yield dense SiC substrates with known shrinkage and sintering characteristics ideal for producing thin or thick SiC layers was developed. The tape consisted of silicon carbide powder, boron carbide powder, a source of carbon, organic solvents, an organic binder, and a plasticizer. SiC tape slurries were mixed and then cast on mylar to yield a dry, thickness of 483 μm/0.019" thick. As described in section 2.2, a sintered thickness of 600 μm is desired. Obtaining this thickness, however, would have required additional effort on modifying the process parameters that would have exceeded the time and resources available in the project to determine a process for making uniform tape of constant thickness. In past projects, Ceramatec has routinely cast tape with a sintered thickness of 600 μm on commercial scale equipment.

Therefore, for consistency of testing and analysis, all the plates made in this project were fabricated from the 483 μm-thick tape. Individual layers of the tape were laminated together, prior to featuring, to provide tape with a thickness that produced 600 μm-tall channels after sintering.

3.1.2 SiC tape lamination and laser featuring – HX plate construction

Following the results obtained in Task 2, a HX plate consisting of five distinct sub-layers, shown schematically in Figure 10, was designed. Each sub-layer is first laminated using baseline-thick tape, with Figure 10 also showing the number of base-thick layers that are utilized in each sub-layer. Heat lamination of sub-layers is accomplished through heat and load. Figure 11 shows a photograph of the press used to load the tapes and bond the layers through applied heat (near 70°C) and load (load may vary, but typically is near 20000 lbs for *non-featured* layers with large surface area).

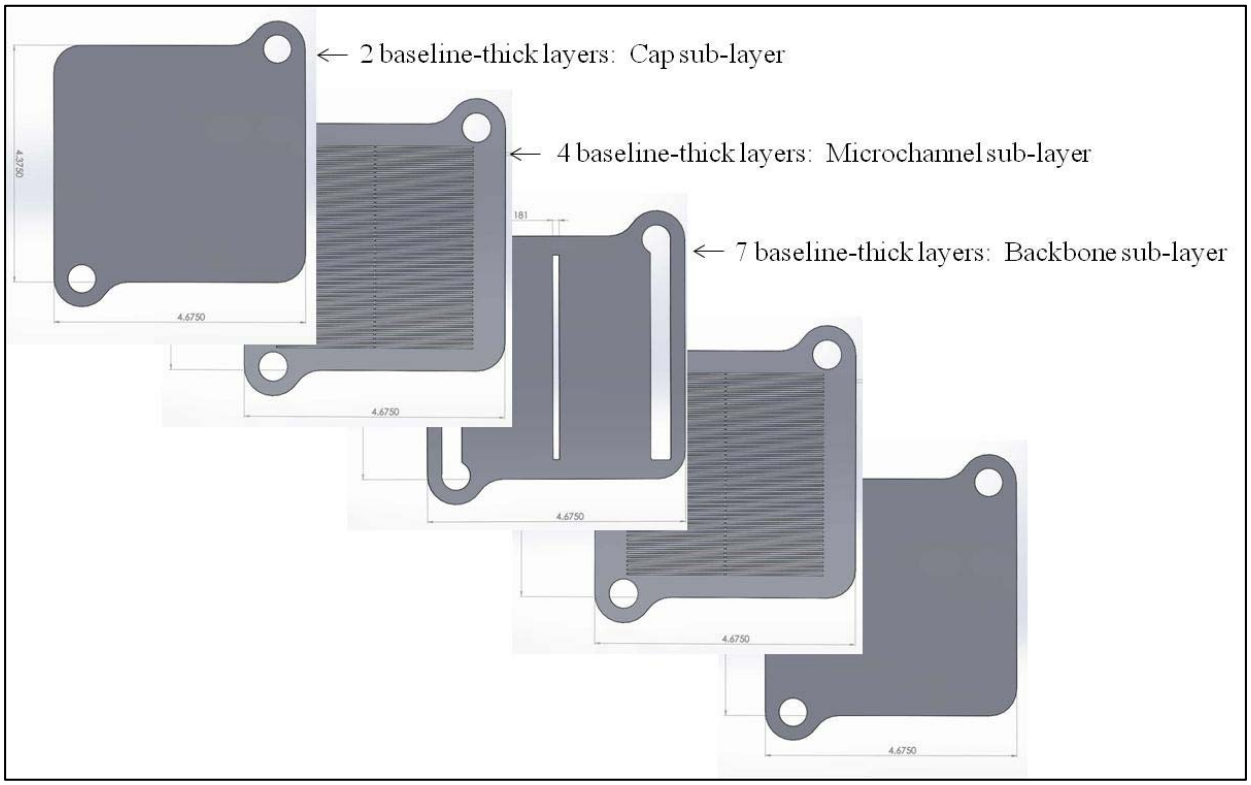

Figure 10 Layered schematic presentation of HX plate, which consists of five distinct sub-layers (microchannel and cap sub-layers are mirrored around the backbone layer). Each sub-layer is first laminated using baseline-thick tape (the number of baseline-thick layers in each sub-layer is shown). Laser featuring of sub-layers occurs later in processing.

Figure 11 Press used to bond the sub-layers through applied heat and load.

Once the sub-layers are laminated, laser featuring is employed to produce the microchannels per design. In addition to the outer periphery, and as seen in the previous Figure 10, the cap sub-layer only has ports lased, but the microchannel and backbone sub-layers have extensive laser featuring to produce the required channels at design dimensions to enable heat exchange functionality in the finished plate. Figure 12 shows the laser station used at Ceramatec that completes this task. After laser featuring, all sub-layers are cleaned to remove any debris generated by laser cutting. Subsequently, each sub-layer is stacked appropriately (noted in Figure 10) and laminated at lower load than used for non-featured layers to prevent distortion of the microchannel features. A fully laminated plate is shown in Figure 13. In addition, ring-shaped spacers, used to provide a gap between the plates in the final heat exchanger stack, are laminated on the port region of the capping layers.

Figure 12 Laser station at Ceramatec utilized to accomplish microchannel featuring of each distinct sub-layer within Design 1.2 heat exchange plates.

Figure 13 Fully laminated plate.

3.1.3 HX plate de-binding and sintering

To enable the handling of tapes during the various levels of processing, the tape formulation requires binders and plasticizers. These organic additives must be removed before the sintering process. The removal of the organic constituents of the ceramic tape is referred to as either debinding or delubing (both used interchangeably). While organics from the binders and plasticizers are removed, debinding in nitrogen allows for intentionaly added carbon sources that are needed in the sintering process for densification and microstructural development purposes to remain.

The individual laminated plates are placed on setters (substrates that ceramic objects are placed on for debinding and sintering). Setter plates are typically chosen to have material chemistry and surface properties that prevent the sintering object from bonding to the surface of the setter plate. The SiC HX plates were debound by heating to 700°C in flowing nitrogen with slow ramp rates that ensure the organics are able to diffuse out of the green structure without any structural damage to the component.

Following the debinding stage, the SiC plates were transferred to a furnace for pressureless sintering in argon ambient. Sintering temperatures to obtain near-theoretical density for these plates are over 2100°C. Theoretical density is 3.21 g/cm^2. The measured density of Ceramatec pressure-less sintered SiC was determined to be greater than 98% theoretical. Figure 14 shows a sintered plate, while Figure 15 shows a side-by-side comparison of a green plate vs. a sintered plate, giving a sense of the shrinkage, approximately 22%, due to sintering. The faying surfaces of the spacers are lightly ground (noted on the sintered spacer in Figure 14) to meet a criterion for surface flatness in preparation for the plate-to-plate joining used in stack assembly. A typical cross-section of the microchannel region of a sintered plate is shown in Figure 16.

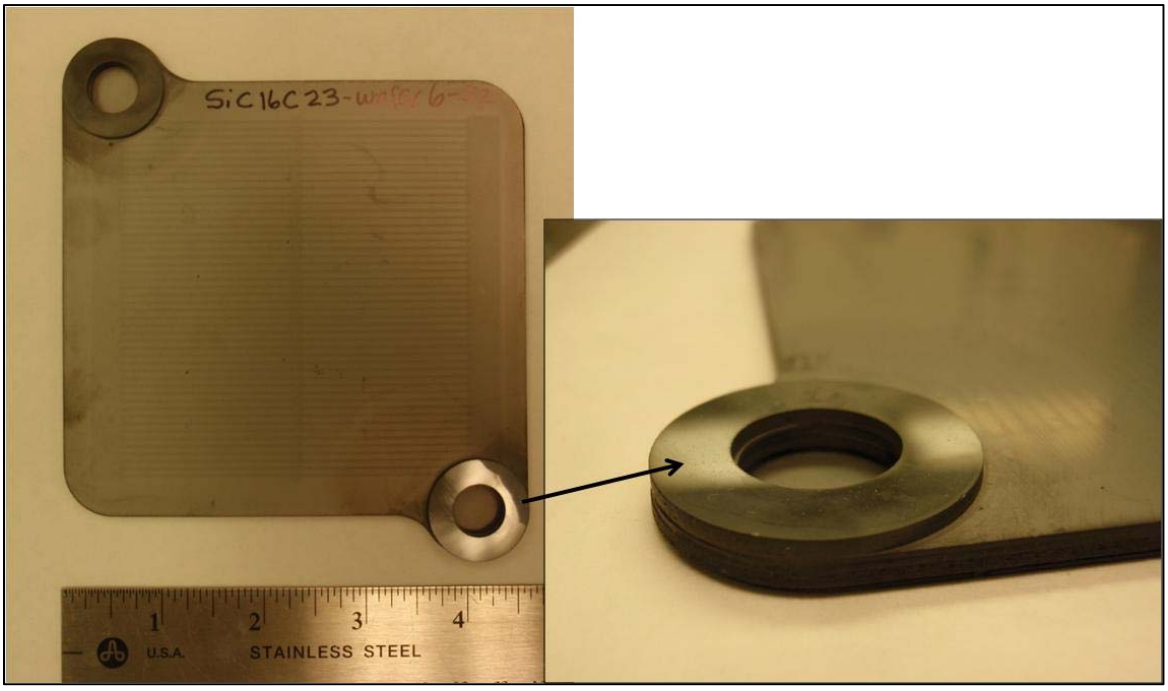

Figure 14 Sintered plate. The co-sintered spacer (applied to all plates and ground to improve flatness after sintering) is shown on the right side of this figure at higher magnification.

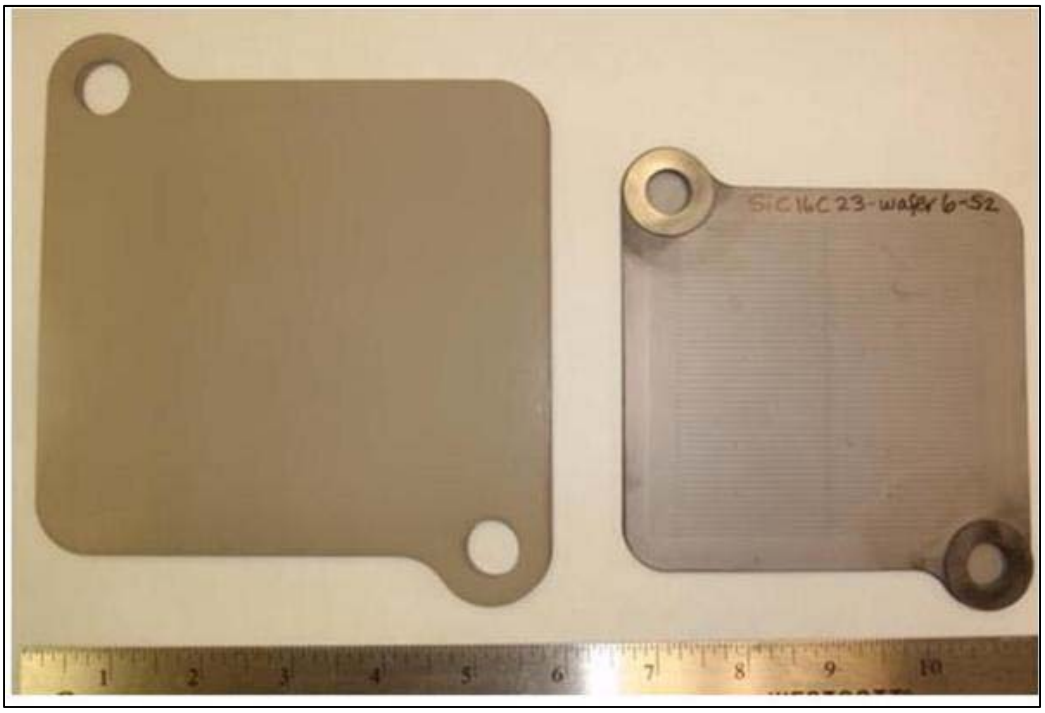

Figure 15 Side-by-side comparison of an unsintered plate (left side) vs. a sintered plate (right side).

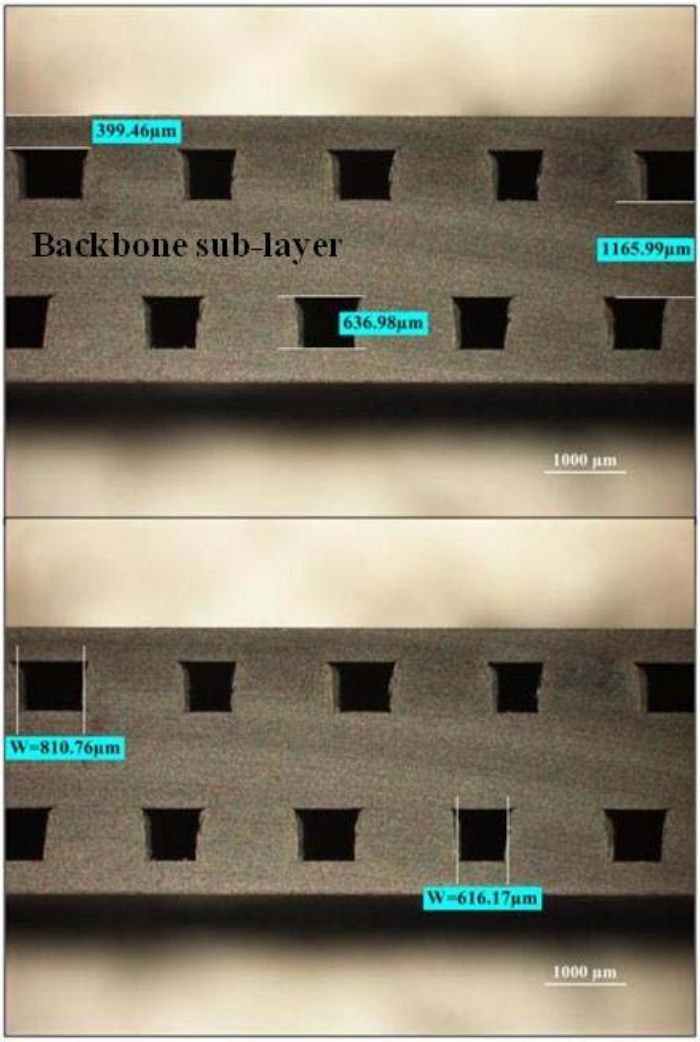

Figure 16 Optical cross-section of a microchannel region within a sintered HX plate. Sintered plate thickness is approximately 3.2 mm, with the outer dense membrane being ~400 µm-thick.

Subtask 3.2 – Thermal / Flow Validation

Validation of flow characteristics of sintered plates was accomplished by placing a sintered plate (shown in Figure 14 on a custom designed flow apparatus seen in Figure 17. Figure 18 shows a side view of a plate being tested. The apparatus allows for variation in mass flow and the ability to use air or custom gases, with appropriate gauges to measure internal plate pressure drop and flow. A single plate is placed on the support platform (b) and tightened down with a top cover to ensure flow through the sintered plate. Plates were tested using air at room temperature.

Results of room temperature air flow testing are shown in Figure 19, where results from an older version (Design 1) plate are included. Design 1 was fabricated in the same way as Design 1.2 (outlined in this report), but it was found that the pressure drop of Design 1 was too high, and hence a redesign of microchannel dimensions was required to provide a dramatic reduction in pressure drop. The results show that the plates used in this project exhibited low pressure drop, as required.

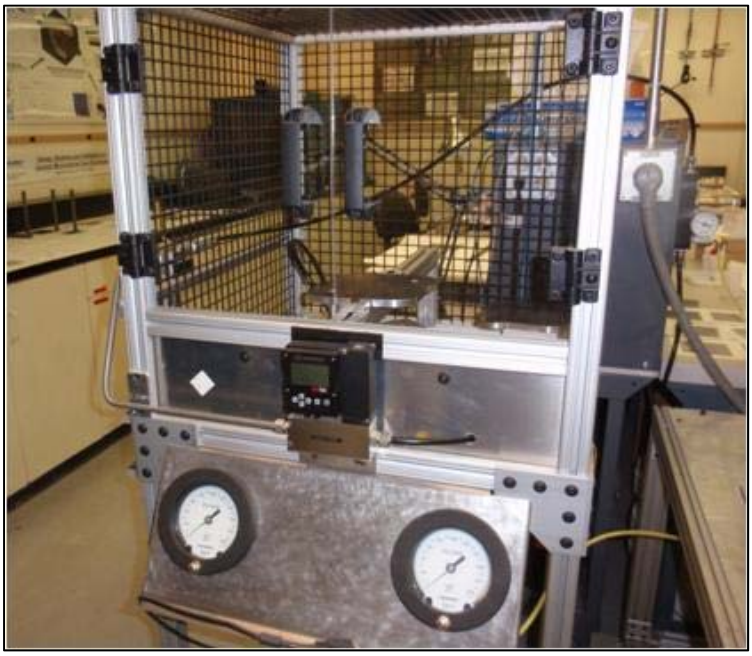

(a)

(b)

Figure 17 Custom designed flow apparatus (a) for testing pressure drop of single sintered HX plates.

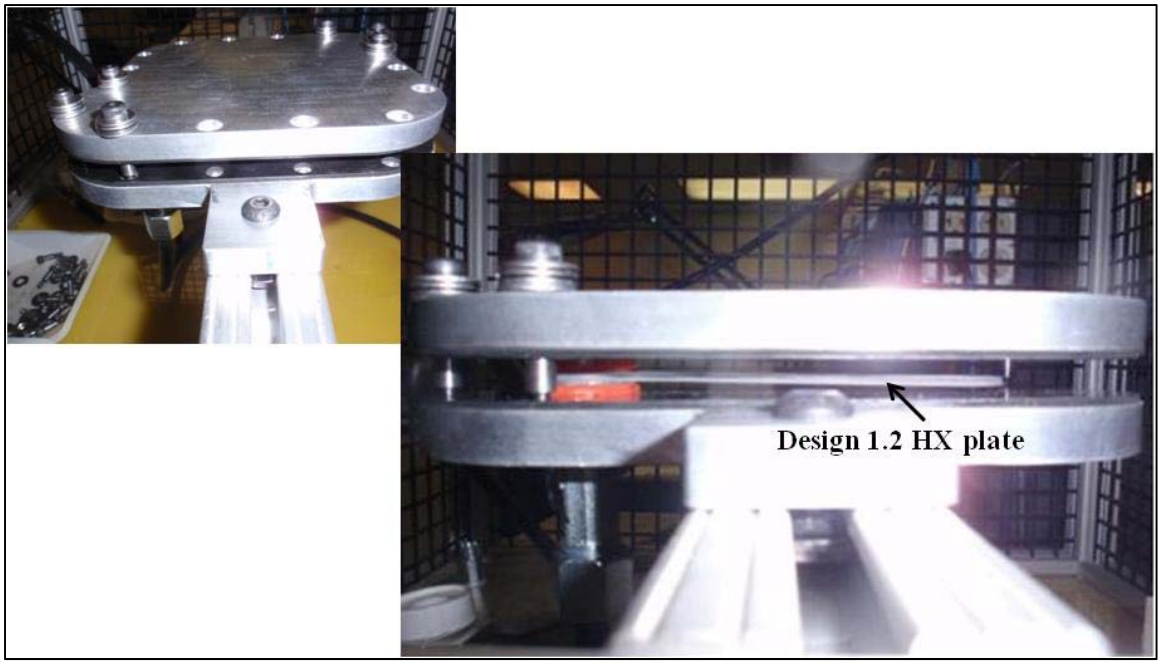

Figure 18 Side view of a plate being tested for pressure drop at various flow rates (air at room temperature).

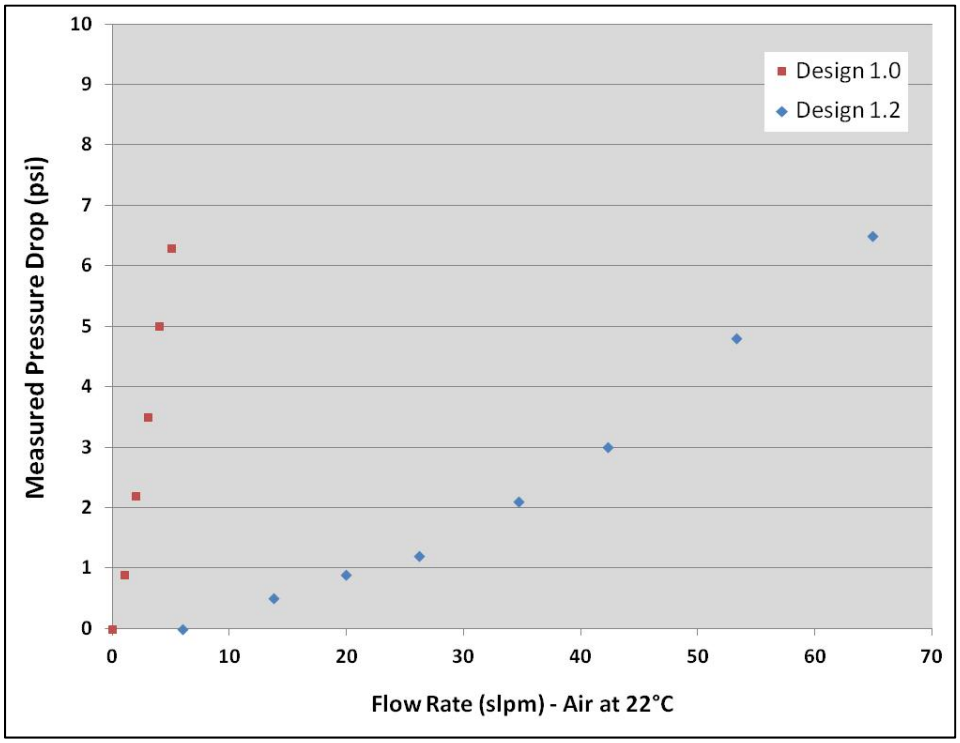

Figure 19 Results of room temperature air flow testing for Design 1 and Design 1.2 sintered HX plates.

Subtask 3.3 – Heat Exchanger Plate Mechanical Evaluation

The mechanical behavior of heat exchanger plates was evaluated in two ways: the allowable pressure differential for a given failure probability was calculated as a function of channel width, and the ten-plate stack was subject to an uncontrolled furnace shutdown to observe its thermal shock resistance. For the allowable pressure calculation, material properties of sintered silicon carbide samples made at Ceramatec with the same starting powder size and sintering profile as used to make heat exchanger plates were used.

To determine the channel width that could support a given pressure differential, each microchannel was modeled as a simply supported beam subject to a uniform, distributed load. The maximum stress induced by the pressure differential was calculated using the well-known, two-dimensional, closed-form solution for beams of increasing length, representing the channel width. The thickness of theheat transfer layer, required to support the pressure, was 1.2 mm. The thermal duty of a plate containing n microchannels was assumed to be v kW. The number of microchannels required for a system with a specific heat duty was calculated by dividing the required system size by the heat duty of a single plate and multiplying by the number of microchannels in a plate. Therefore, for a 1 MW system, if a single plate performed a heat duty of 1 kW and contained 100 microchannels then 100 000 microchannels would be required. If the system failure rate was desired to be 1×10^{-6}, then the failure rate of an individual channel in that system had to be 1×10^{-11}.

Weibull statistics were used to determine the allowable channel width. A Characteristic Strength of 587 MPa and a Weibull modulus of 6.4, obtained from measurements of material described above using ¼ four-point flexural testing was used in the two-parameter Weibull analysis. A spreadsheet was used to determine the failure probability as a function of channel width (beam length). The spreadsheet calculated the maximum stress in the beam, due to the pressure differential, for a given beam length and then calculated the failure probability of a beam that size using Weibull statistics.

Results for the allowable channel width as a function of system size (number of microchannels) and pressure differentials is shown in Figure 20. The lines in Figure 20 represent the maximum width that a channel could be to support the stress induced by the pressure differential for a given system size. For example, for a 100 kW heat exchanger (0.1 MW), the channel width could be as wide as 2.5 mm if the maximum pressure differential was 50 bar; 1.1 mm, 300 bar. Since these pressures are well above those encountered in a microturbine, the analysis shows that the design of the heat exchanger selected should be very reliable under steady state operating conditions and even for large pressure upsets. The results show that, for the system failure rate chosen, 1×10^{-6}, a maximum channel width of 0.6 mm could be used in systems as large as 1 MW under 300 bar pressure. Since it is preferable to limit the channel width to >0.6 mm for pressure drop requirements, if larger systems or pressure differentials were required, the thickness of the heat transfer layer could be increased, or a material with higher strength used.

A test that was performed to evaluate the mechanical durability of the plates was subjecting the 10-plate stack to an uncontrolled furnace shutdown to observe its thermal shock resistance. At stack undergoing testing, as will be described later, was held in a furnace at 800°C with 60 lpm of air flowing over the plates and 60 lpm of air flowing through the plates (in microchannels). The furnace was shutoff to simulate an unplanned turbine trip, although no pressure was applied as there would be in an actual turbine. At the start of the transient, the hot side of the plate was approximately 896°C; the cold side, 718°C. The microchannel inlet was 173°C (there is some air preheating in the ceramic tube feeding the microchannel plates); the outlet, 800°C. Notice the large temperature gradient supported across the plates, as well as the gradient through the thickness of the plates. The time constant for cooling was about 4 hours, so in the first ten minutes of cooling the temperature dropped about 50°C. After this test the stack was

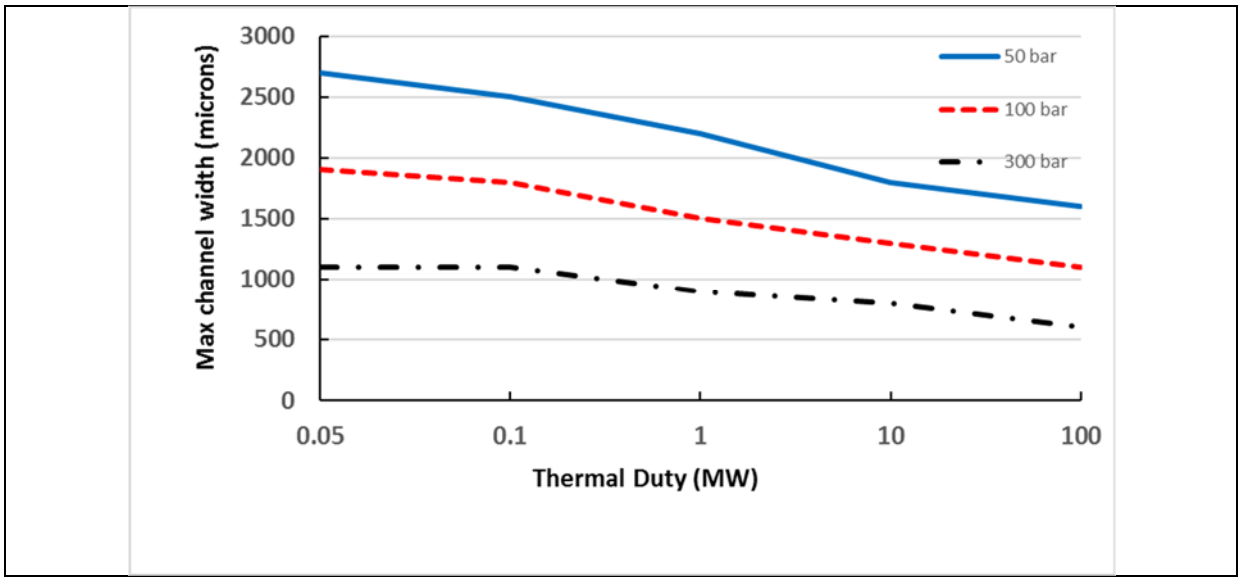

Figure 20 Maximum channel width capable of providing a system failure probability of 1 x 10-6 as a function of system thermal duty and applied pressure differential.

intact fully and leak tight. Although the cooling rate was not that fast, the stack would have been subject to some relatively high thermal stresses due to the non-linear and transient thermal gradient. A recommendation for follow-on work would be to model the steady state and transient stress states of stacks to further estimate reliability and determine operating conditions.

Task 4.0 – Prototype Stack Fabrication

4.1 Leak testing and qualification of individual sintered HX plates

For quality control, the leak rates of individual sintered HX plates used to assemble HX stacks were measured to provide an indication of whether there were any defects that would reduce efficiency or reliability. Both qualitative observation and quantitative measurements obtained through helium leak testing and vacuum decay were used. A leak testing plate was developed to quantify leakage. Figure 21 shows the leak testing support unit used for both helium leak and vacuum decay testing. The quantification of both helium leak rates and vacuum decay for a given HX plate provides the needed bridge to understand the qualitative results observed in associated bubble testing. All leak testing results were uploaded into the processing data base.

Low leak rates were obtained (hermetic yield > 50%). The leak rates for all plates used in the prototype, 10-plate SiC HX stack discussed in this report are shown in Table 8. It is important to note, as seen in Table 8, the vacuum decay leak rate measurement (as obtained by Ceramatec's vacuum decay device) is not able to measure differences in leak rates for samples with less than 0.003 sccm, broadly corresponding to helium leak rates of 10^{-6} sccm and lower. Additionally, it is also worth noting that plates which did exhibit leakage, relative to hermetic levels, had leakage associated only with the spacer gasket-to-wafer interface, with Figure 22 showing a bubble test photograph of gasket-to-wafer leakage at a leak location. Bubble tests are a very important tool to identify the location of leaks and the qualitative nature of that leak to assist in process improvement to prevent introduction of this defect in future processing. For all plates tested, no leaks were observed between laminated tape layers (layer to layer, or outer dense cap membrane) suggesting that the lamination process and tape quality was sufficient for plate processing.

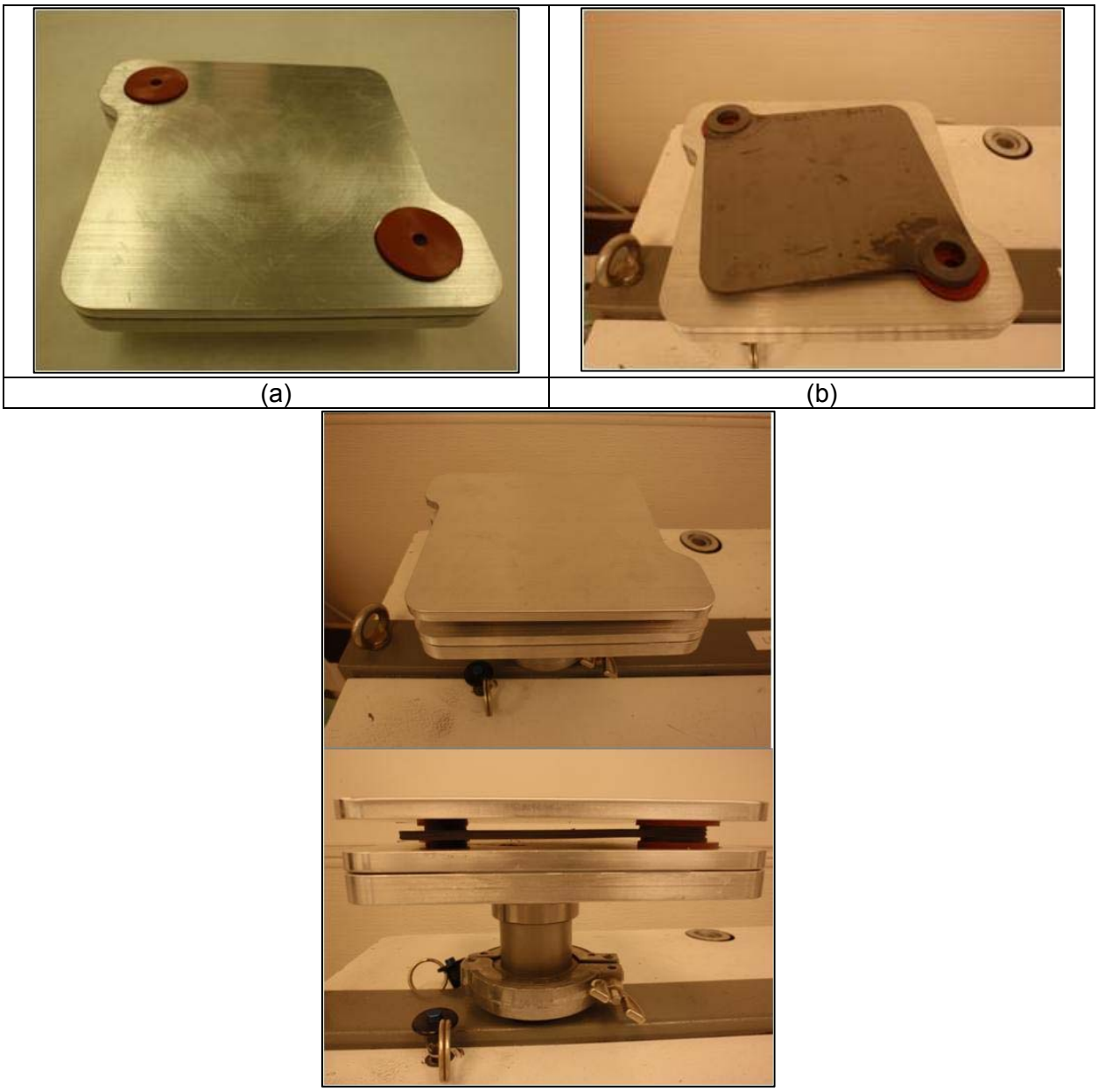

Figure 21 Leak testing support device to quantify leakage in SiC HX sintered plates: a) support plate only, b) with sintered HX plate in place, c) cap placed over the HX plate and in position on the helium leak tester. This same aluminum support device is used for vacuum decay tests.

Table 8

Leak testing data and observations for all Design 1.2 plates used in the prototype 10-plate SiC HX stack discussed in this report.

HX Plate ID	Helium Leak Test	Vacuum Decay	Bubble Test Observations
	Leak Rate (sccm He)	Leak rate (sccm, at 30 seconds)	at 15 psi pressurization
SiC16C23-wafer7-S3	$1x10^{-8}$	0.003	none observed
SiC16C23-wafer1-S4	$3x10^{-6}$	0.003	none observed
SiC16C23-wafer2-S5	$3x10^{-5}$	0.005	none observed
HeatEX-ETR-001-wafer2-S1	$4x10^{-3}$	0.117	Small - spacer gasket
HeatEX-ETR-001-wafer4-S2	$2x10^{-8}$	0.003	none observed
HeatEX-ETR-001-wafer5-S3	$4x10^{-7}$	0.003	none observed
HeatEX-ETR-001-wafer6-S4	$2x10^{-8}$	0.002	none observed
HeatEX-ETR-001-wafer7-S5	$1x10^{-2}$	0.204	Large - spacer gasket
SiC16C23-wafer3-S1	$2x10^{-8}$	0.003	none observed
SiC16C23-wafer4-S2	$2x10^{-8}$	0.003	none observed

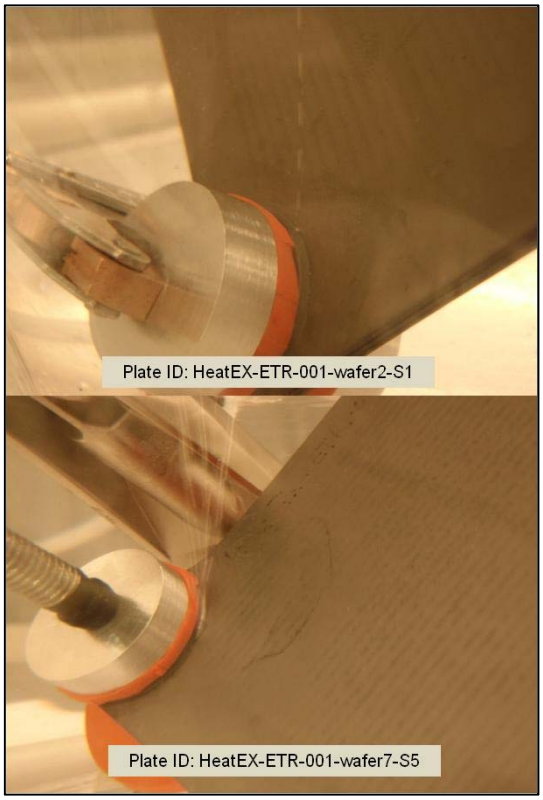

Figure 22 Bubble test photographs showing leakage at the spacer-to-wafer interface region. Compare bubble leak images to the associated leak data in Table 8.

4.2 Prototype SiC HX sub-module stack assembly

Ten, individual microchannel HX plates were stacked with two 0.75” OD x 0.50” ID SiC tubes (inlet and outlet flow tubes) placed on the inlet and outlet ports. Bonding material was applied between the spacer of one plate and the joining surface of the next and between the SiC tubes and the inlet and outlet ports. Figure 23 shows a completed stack prior to joining and the arrangement of external load plates used to apply a static load during the joining process. The assembly was heated, in air, using a controlled thermal profile. Bonding was accomplished at approximately 1200°C. After joining, the stack was removed, and is shown in Figure 24. A qualitative bubble test was performed on the entire tube-to-stack assembly to evaluate the quality of bonding. Observationally, only minor hairline bubbles were seen at a few joints. At this processing stage of development, a full stack (with joined tubes) was not quantitatively leak tested but only qualitatively observed since the set up and needed support structures for large multi-plate stack quantification of leakage must still be designed and machined for use.

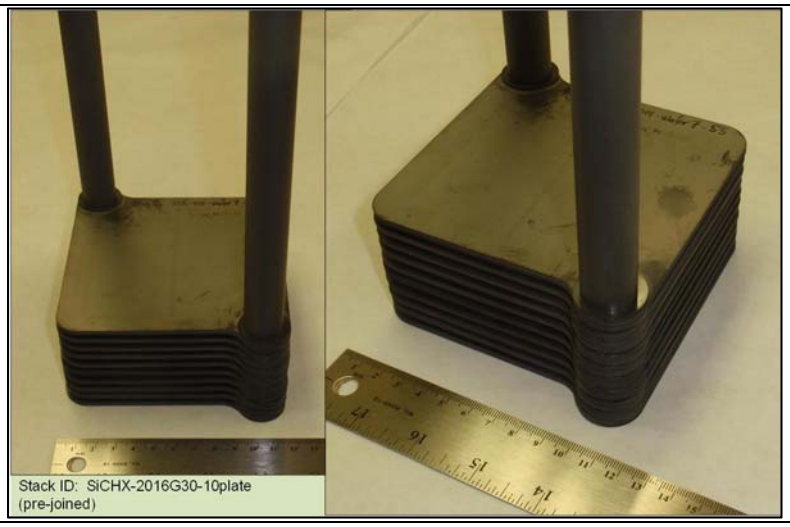

(a)

(b)

Figure 23 Pre-joined 10-plate SiC HX stack, with (a) inlet and outlet flow tubes, and (b) furnace set-up and stack placement for joining.

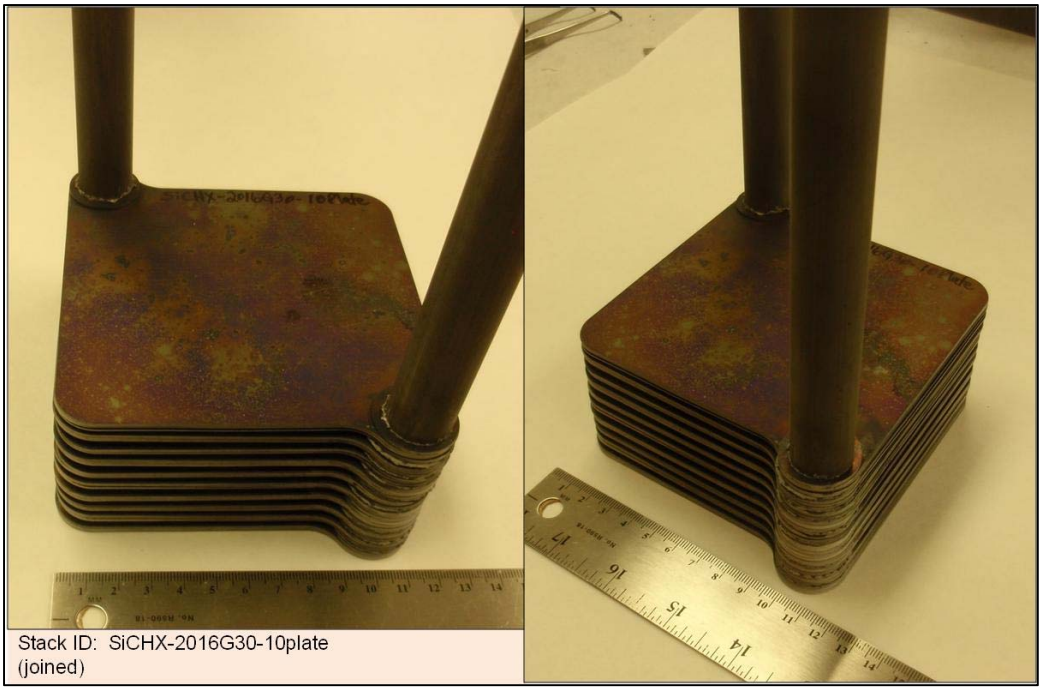

Figure 24 Fully joined 10-plate SiC HX stack (with inlet and outlet flow tubes).

Task 5.0 – Prototype Stack Testing

5.1 Test Apparatus

Several single-plate and three-plate stacks were joined with inlet and outlet tubes (tubes are seen in Figure 24) for pressure drop and thermal performance measurement purposes and also for subsequent assistance in preparing a thermal test apparatus for prototype, 10-plate stack testing. Using high temperature furnace refractory panels, a flow box for high temperature 10-plate stack testing was developed as seen in Figure 25. The flow box was placed inside a resistively heated furnace that provided the heat source for testing. Figure 26 shows side views of the flow box, which includes (in the back) a smaller alumina gas pre-heater. The alumina pre-heater (heated directly from the larger box furnace ambient) has a porous interior to increase surface area to more effectively heat the incoming air directed from the outside of the furnace. After some basic testing of this alumina pre-heating unit, it was found that it failed due to extreme thermal gradients in the pre-heater itself. As a result, a coiled (10.5 linear feet) 304 stainless steel pre-heater replaced the alumina pre-heater as shown in Figure 27.

Installation of a single plate, joined to inlet and outlet tubes, is shown in Figure 28, illustrating how a stack is placed into the flow box and sealed in place for testing. The joined 10-plate stack (refer to Figure 24) was placed into the flow box, and is seen in Figure 29. This same figure shows the air flow configuration and directionality for internal stack flow and over-the-plate flow, with thermocouple placement for temperature measurement in operation. For flow designation purposes, air flow that moves internally within the HX stack is referred to as ‘HX stack inlet’ and ‘HX stack outlet’ flow. The air flow that moves over the plate (pre-heated air from the heating coils) enters in the smaller flow box on the right side window and flows over the plate. Thermocouples measure the temperature of the pre-heated air just before it flows over the plate and is referred to as ‘Over-the-plate Inlet Window’. The air that has just completed flowing over the plates and is exiting the flow box through a window on the left side of the box (with thermocouples present to measure the temperature) is referred to as ‘Over-the-plate Outlet

Window', with this air flowing out the back of the flow box and out of the larger furnace via an exhaust pipe that further allows for outside-of-the-furnace cooling.

The 10-plate stack inside the flow box was placed into the furnace for testing, as shown in Figure 30. This same figure shows ports for HX stack inlet flow, outlet flow, and pressure drop measurement. Figure 31 shows a schematic representation of where the thermocouple junction is located within the 10-plate HX stack to better understand where the HX stack inlet and outlet temperature measurement is taking place. This junction is located on the joint plane of the spacer-to-tube joint region on the top most HX plate of the stack. Figure 32 shows a picture of the overall testing station where data from stack performance is collected. Testing of heat exchange performance for the10-plate stack was performed at various stack flows, over-the-plate flows, and various temperatures.

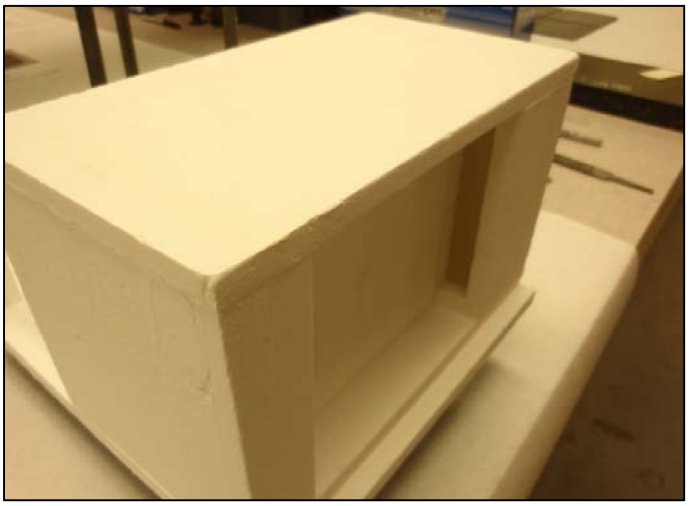

Figure 25 High temperature furnace flow box (made of furnace refractory panel material) for high temperature 10-plate stack testing.

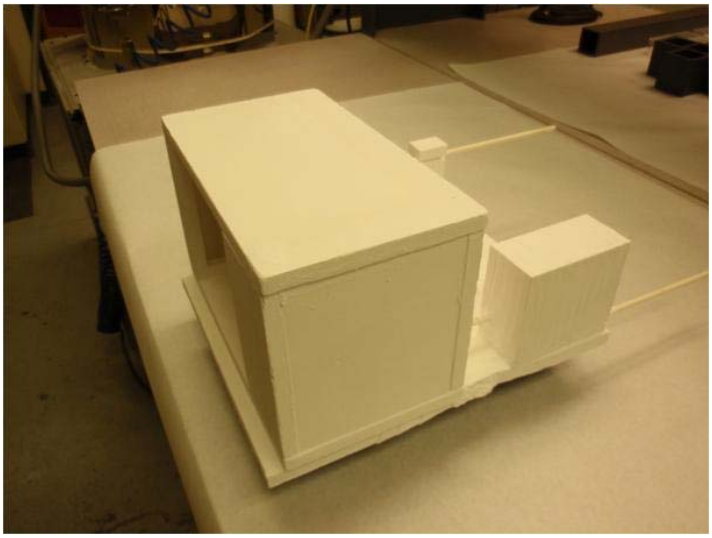

Figure 26 Side view of the test box insert platform, which includes (on the right of this image) a smaller alumina gas pre-heater Pre-heated inlet gas enters on the right side flow box, while outlet gas exits the test box through the outlet tube on the upper right of this image.

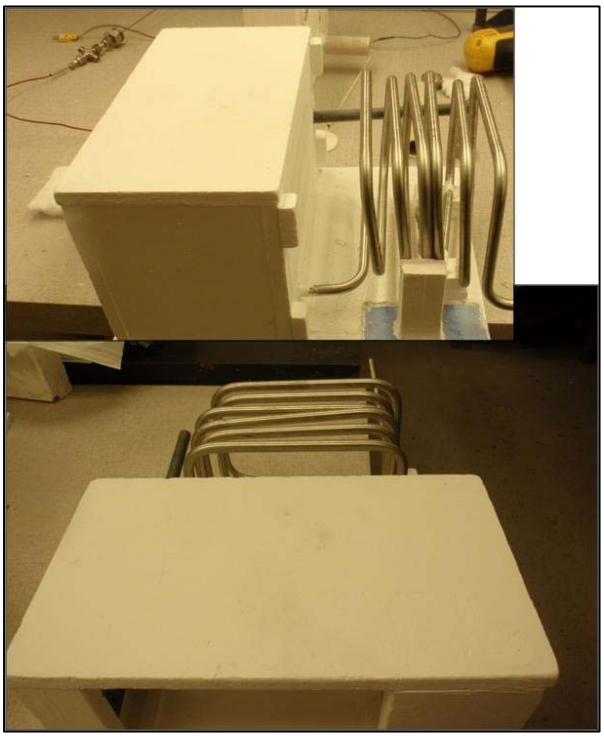

Figure 27 Coiled (10.5 linear feet) 304 stainless steel pre-heater replacing the alumina pre-heater unit.

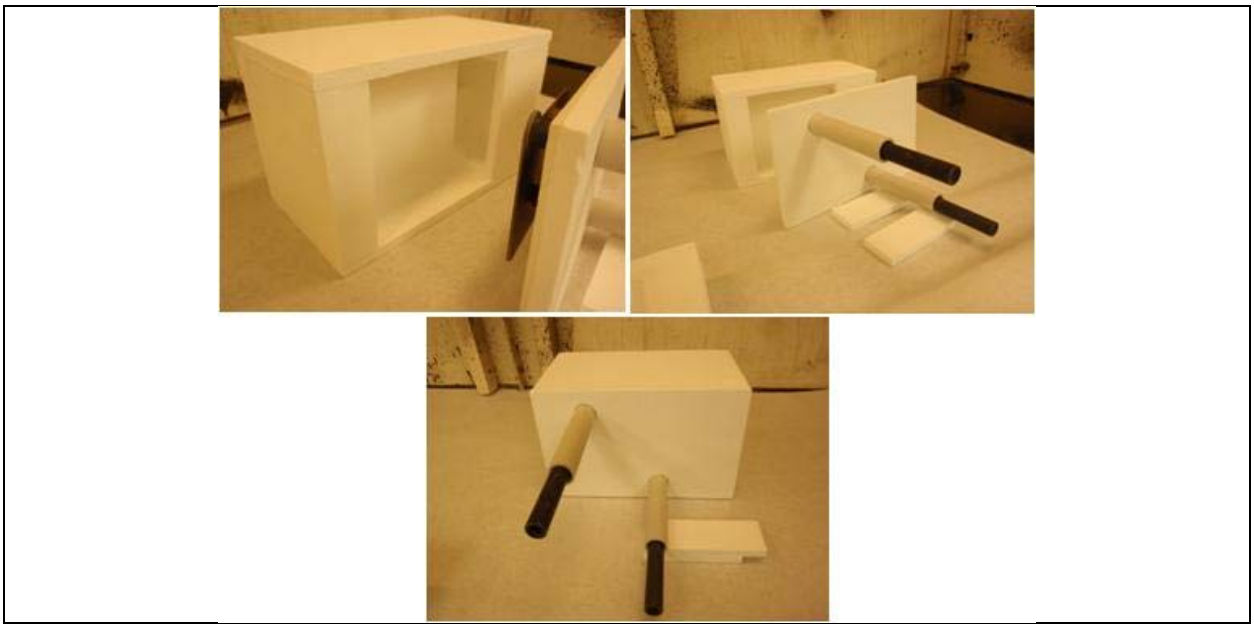

Figure 28 Demonstration of how a heat exchanger stack, using a single plate (joined to tubes), is placed into the front door of the test box and sealed in place for flow testing.

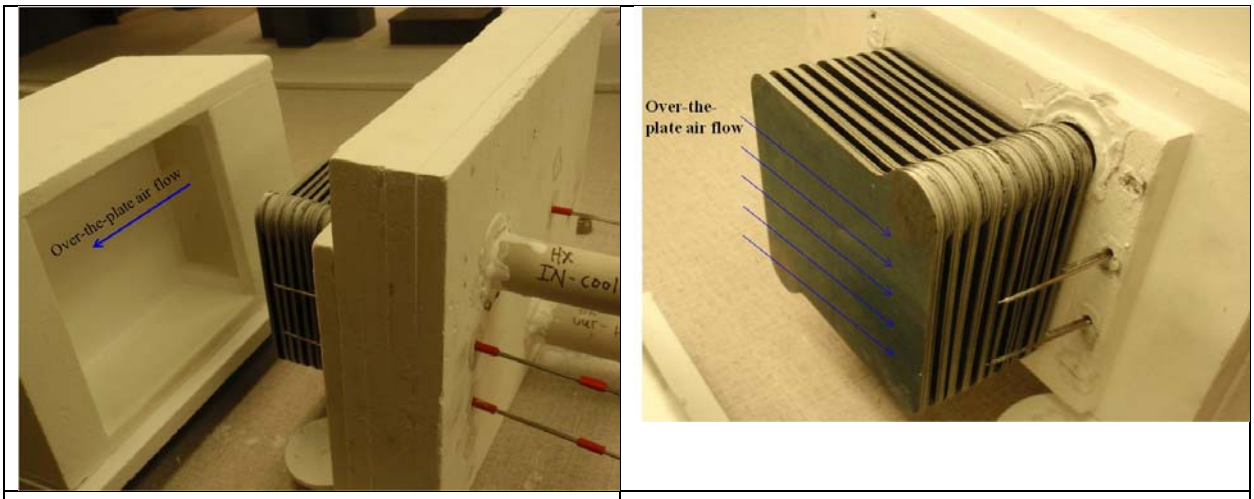

(a) (b)

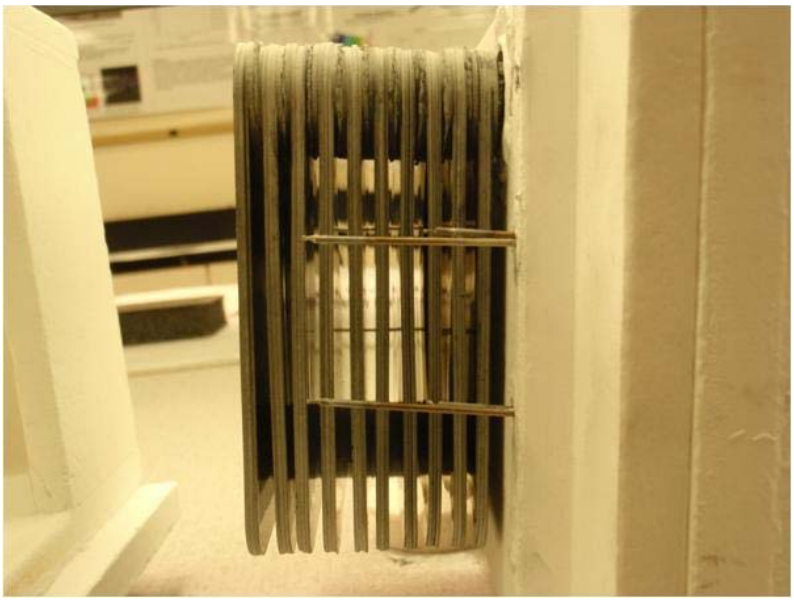

(c)

Figure 29 Picture of the 10-plate stack placement within the front panel of the flow box. Air flow configuration and directionality for internal stack flow and over-the-plate flow, with thermocouple placement for temperature measurement in operation are shown here, with (a) showing flow box air flow and HX plate inlet and outlet flow ports and basic thermocouple placement as seen from the outside panel, (b) showing an angled view of the 10-plate stack in place and over-the-plate air flow directionality and thermocouple placement (with thermocouples identically placed on the front end the same as shown here on the back end, and (c) shows a side view of the 10-plate stack before it is sealed into place within the flow box.

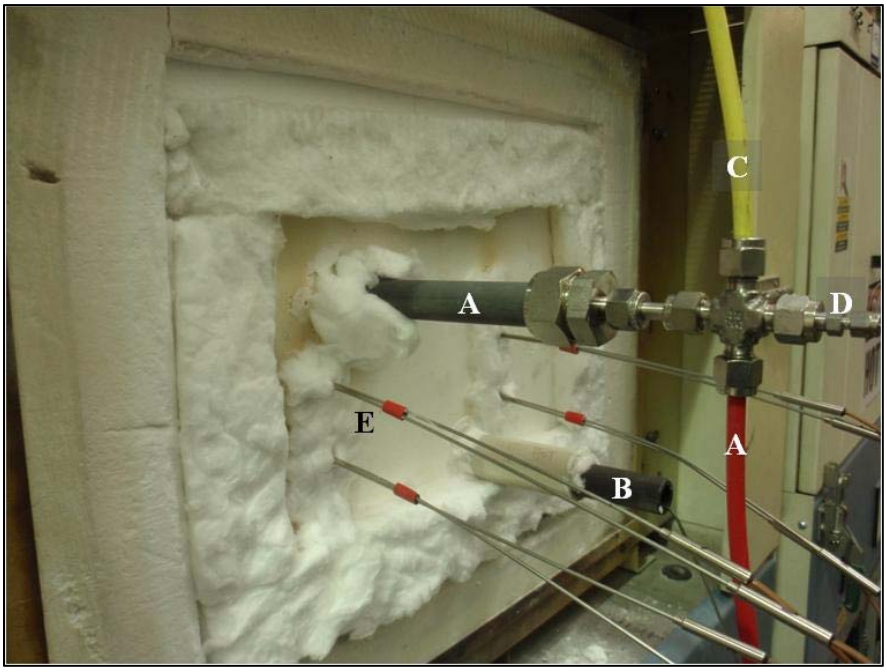

Figure 30 Photograph of the 10-plate stack flow box set into the furnace ready for testing. This same figure shows ports for HX stack inlet flow, outlet flow, and pressure drop measurement, with A) HX plate inlet gas, B) HX plate outlet gas, C) pressure port for HX plate pressure drop measurement, D) thermocouple to measure HX plate inlet gas temperature (plate outlet has a similarly place thermocouple, and E) one of several variously placed thermocouples that measure over-the-plate inlet and outlet window temperatures.

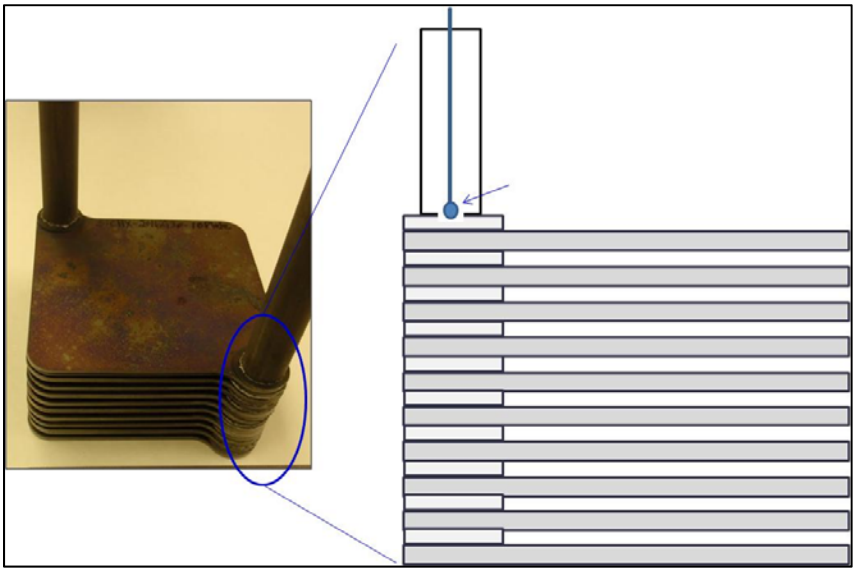

Figure 31 Schematic representation of where the thermocouple junction is located (noted by arrow) within the 10-plate HX stack to better understand where the HX stack inlet and outlet temperature measurement is taking place.

Figure 32 Testing station where data from stack performance is collected.

5.2 Test Results

A total of four prototype stack tests were performed. Two tests were performed on a three-plate stack and two on a ten-plate stack. The first test on a three-plate stack involved heating the inlet air to slightly above 400°C, cooling the furnace and stack, and then reheating to 400°C. The results are shown in Figure 33. The test showed that the apparatus, including the connections from the metal supply lines to the ceramic heat exchanger (outside the furnace), worked as planned. Analysis of the results, however, indicated that the measured pressure drop is one order of magnitude higher than the values estimated values from a laminar flow model assuming equal flow in the 34 channels. A significant portion of the higher pressure drop was due to the contribution from the inlet and outlet manifold tubes. Therefore, although the predicted values were not measured, the microchannel stack itself was anticipated to have low pressure drop.

Subsequent CFD analysis, using Star CD, indicated poor air flow distribution within the microchannels, see Figure 34. Modeling suggested that all the air flowed through only a few channels. Using the laminar flow to model flow through a plate with only a few channels, the hypothesis of poor flow distribution was verified. It was realized that since the test conditions were substantially different from the design conditions (i.e. the lab conditions of pressure and flow were substantially different from those in a microturbine) that the flow distribution channel that directed gas flow from the plate ports to the and from the microchannels was too narrow for the test conditions. After verifying that a wider flow distribution channel could be fabricated without impacting leak rate or plate flatness, the ten-plate stack was made with a wider manifold. This is the design referred to throughout this report.

As described above, a stack of ten HX plates was assembled for testing. Two tests were performed on the stack, although it was not removed from the test apparatus between tests. The first test involved heating the stack in the furnace with an internal air flow rate of 20 lpm. A conservative heating and cooling rate of 1°C/min was used. The furnace temperature was varied according to the values shown in Table 9. Temperatures were held at each condition for at least

5 hours to obtain thermal equilibrium. The results of the test are shown in Table 9 and Figure 35.

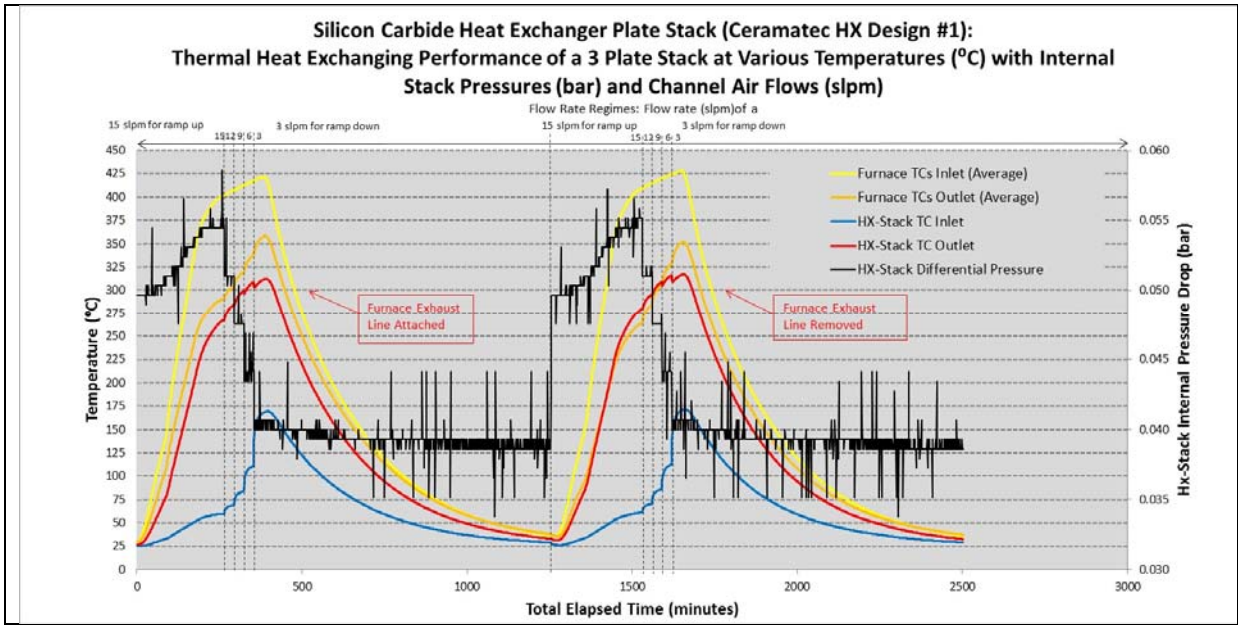

Figure 33 Results from Initial test of three-plate stack.

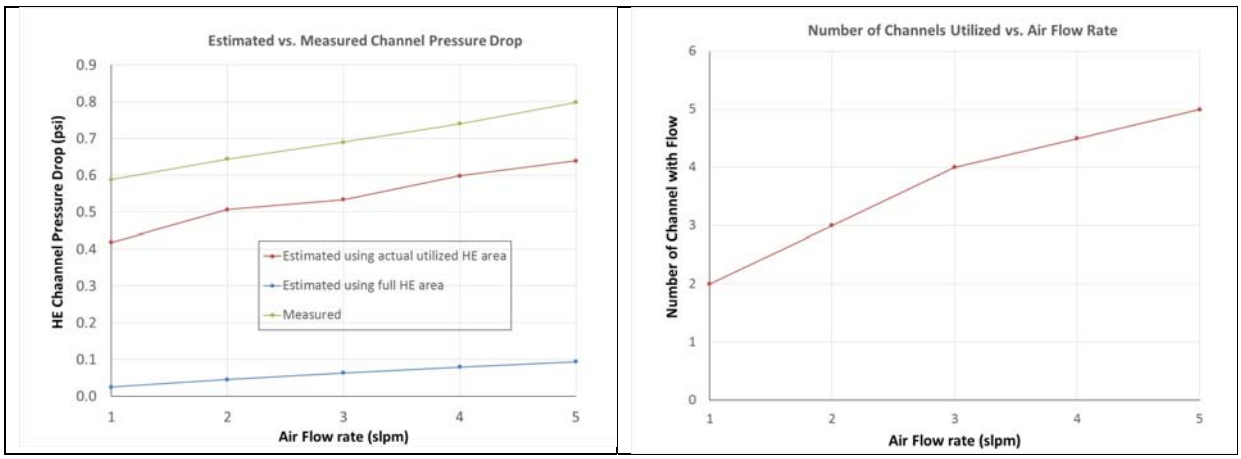

Figure 34 Calculated and measured pressure drop from initial three-plate HX testing.

The results were very encouraging. First of all, it was demonstrated on a modular scale that ceramic, microchannel devices could perform high temperature heat exchange at temperatures above where metal alloys could operate (i.e. > 850°C). Furthermore, high inlet approach temperatures were obtained: indicating very high efficiency. The calculated efficiency was 86%. In addition, very low pressure drops, which included the contribution from the inlet and outlet tubes, were measured: 14 kPa. Although unplanned, the test ended when a breaker limiting the current drawn by the furnace heating elements tripped. Despite the rapid thermal transient, the stack survived and was used for further testing.

The test results were used to extrapolate to the conditions experienced in the microturbine system (c.f. Figure 1) by fitting the heat transfer behavior observed in the laboratory conditions to the output of the laminar flow CFD model and then scaling the gas flow rates. The

Table 9

Furnace Ambient - Hold Segment Temperature °C	Stack Flow / Over-the-plate Flow (slpm)	Over-the-plate Inlet Window °C (average)	Over-the-plate Outlet Window °C (average)	HX Stack (microchannel) Inlet Air °C (average)	HX Stack (microchannel) Outlet Air °C (average)	Thermal Gradient °C: Difference between HX Stack Outlet vs. HX Stack Inlet	Measure Stack Pressure Drop (ps
850	20/20	771.0	686.2	260.4	657.0	396.6	1
1050	20/20	937.1	857.9	396.3	853.9	457.6	1
850	30/30	745.8	635.1	198.8	645.1	446.3	1
1050	30/30	920.0	801.9	296.5	833.8	537.3	1
1050	20/20	930.4	846.8	381.7	851.3	469.6	1
850	20/20	746.2	658.8	250.8	652.5	401.7	1
850	30/30	748.1	642.1	211.4	650.7	439.3	1
850	40/40	754.5	613.4	167.7	652.0	484.3	2
1050	40/40	925.1	771.6	227.2	836.1	608.9	2
850	50/50	757.0	589.0	125.3	644.2	518.9	4
1050	50/50	923.7	731.2	158.5	819.8	661.3	4
1100	**50/50**	**975.2**	**785.5**	**186.0**	**885.6**	**699.6**	4
1100	40/40	968.8	815.1	251.2	886.2	635.0	2
1100	30/30	954.3	827.7	294.1	871.3	577.3	1

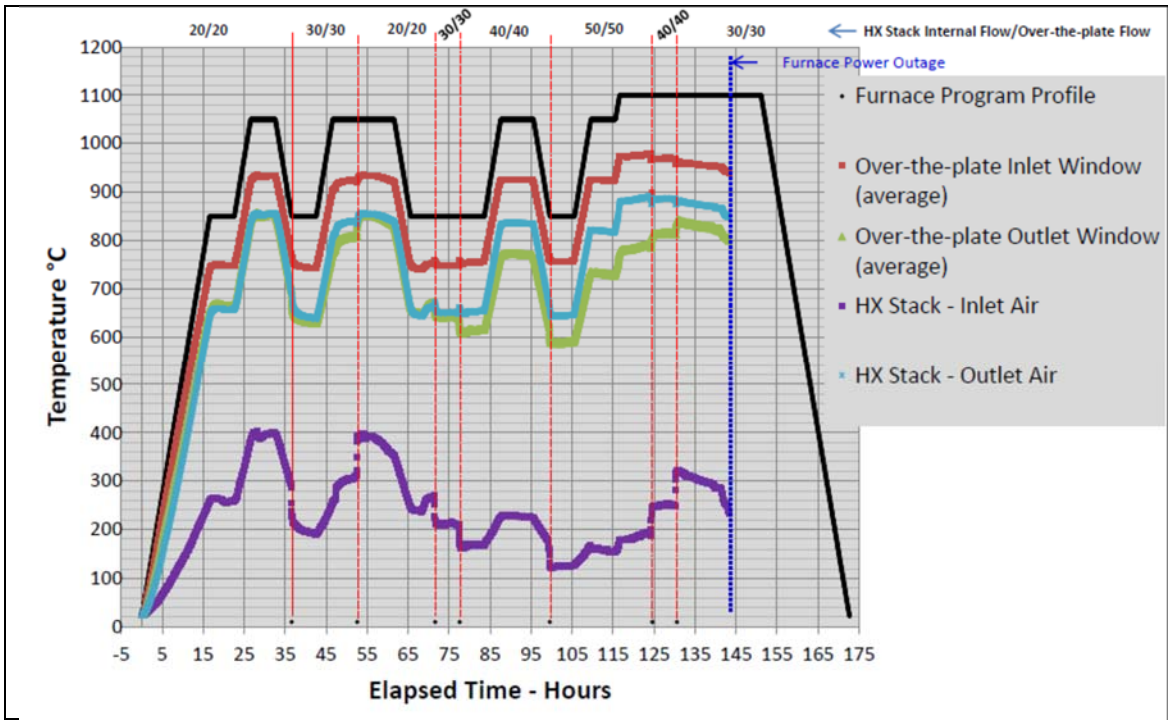

Figure 35 Results of initial test on 10-plate stack. Values at the top of the plot indicate the gas flow rate through the microchannels/across the plates in lpm.

Table 10

Measured and extrapolated HX performance metrics

Case	Experimental	30 kW microturbine	65 kW microturbine	200 kW microturbine
Air flow rate (slpm)	20	15000	25000	75000
Effectiveness	86%	(≥86%)	(≥86%)	(≥86%)
Extrapolated Thermal Duty	200 W (measured)	150 kW	250 kW	750 kW
Pressure drop (kPa)	14	TBD	TBD	TBD

extrapolated results are shown in Table 10. The results indicate that the design is adequate for providing the required heat transfer, assuming that modules of plates identical to those tested in this project are used.

Given the success of the initial test on the ten-plate heat exchanger stack, a second test was performed under additional conditions. This test was performed at a single temperature with varying flow rates, as shown in Table 11. Test results are shown in Figure 36. The results of the second test confirmed those of the first, including that heat exchanger stacks could be cycled between room temperature and high temperature without loss of performance, even if cooling was uncontrolled. The thermal duty of the stack increased as the gas flow increased. With the constraints on the test apparatus, the maximum thermal duty was 800 W, see Figure 37. Since the heat exchanger plates were designed to perform a thermal duty of approximately 500 W each, a flow rate slightly less than one order of magnitude higher is required to verify that the heat exchanger stack can provide 5 kW of thermal duty. Nevertheless, it was confirmed that the design had a high effectiveness, as shown in Figure 38.

Table 11
Test Conditions for 10-plate Heat Exchanger Test #2

Furnace Ambient - Hold Segment Temperature °C	Stack Flow / Over-the-plate Flow (slpm)	Over-the-plate Inlet Window °C (average)	Over-the-plate Outlet Window °C (average)	HX Stack (microchannel) Inlet Air °C (average)	HX Stack (microchannel) Outlet Air °C (average)	Thermal Gradient °C: Difference between HX Stack Outlet vs. HX Stack Inlet	Measured Stack Pressure Drop (psi)
1000	50/50	875.6	693.3	154.2	763.2	609.0	4.
1000	50/40	857.8	672.2	141.2	731.2	590.1	4.
1000	50/30	812.7	642.8	124.9	658.7	533.8	4.
1000	50/20	770.7	607.1	105.1	589.3	484.2	4.
1000	50/10	731.3	582.2	104.7	551.8	447.2	4.
1000	50/0	634.6	570.9	86.8	464.3	377.5	4.
1000	30/30	882.4	770.1	286.0	797.7	511.7	1.
1000	40/40	880.9	724.1	201.2	784.7	583.5	2.
1000	50/50	896.0	718.0	173.1	800.1	627.0	4.

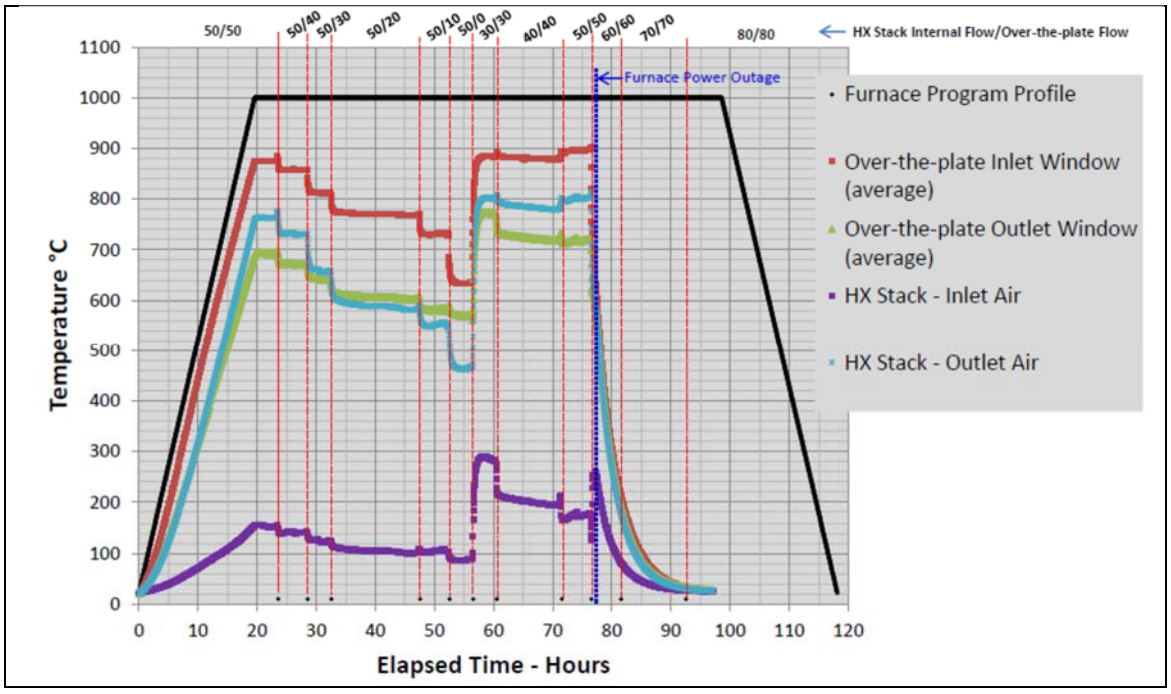

Figure 36 Results of second test on 10-plate stack. Values at the top of the plot indicate the gas flow rate through the microchannels/across the plates in lpm.

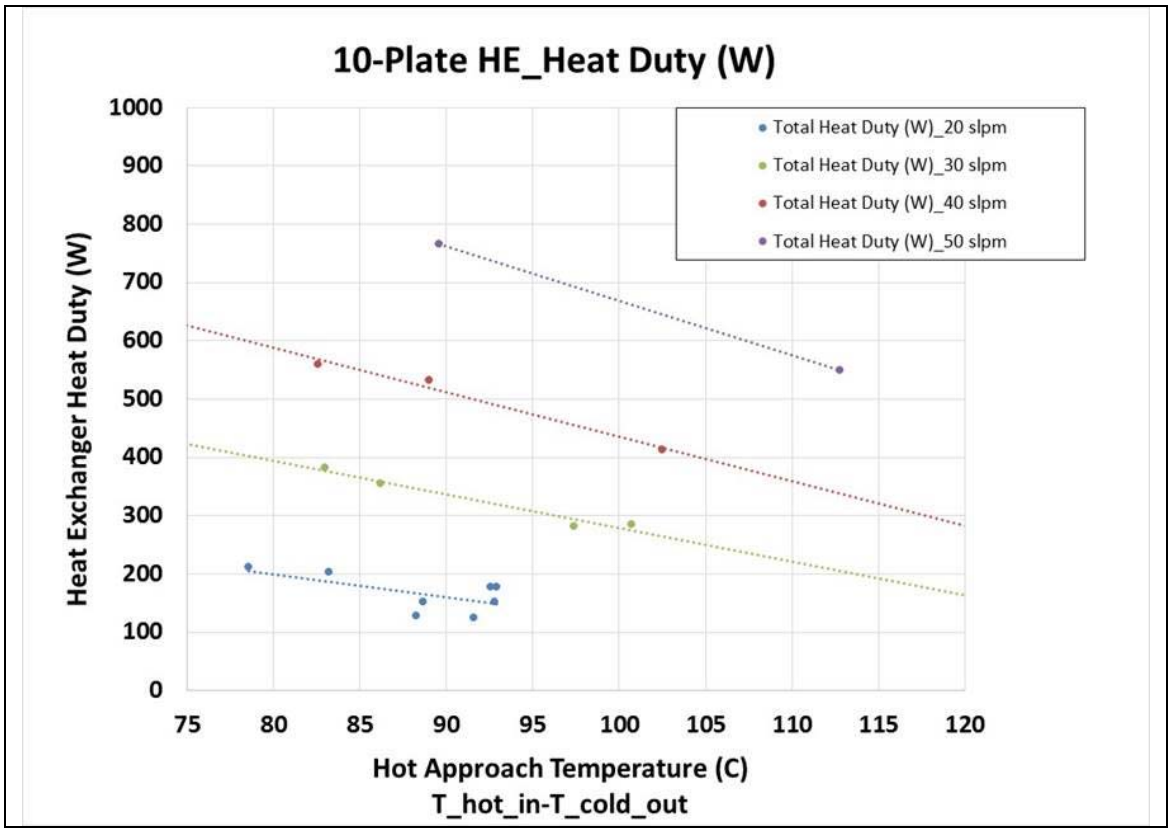

Figure 37 Calculated thermal duty of the ten-plate stack during the second test campaign.

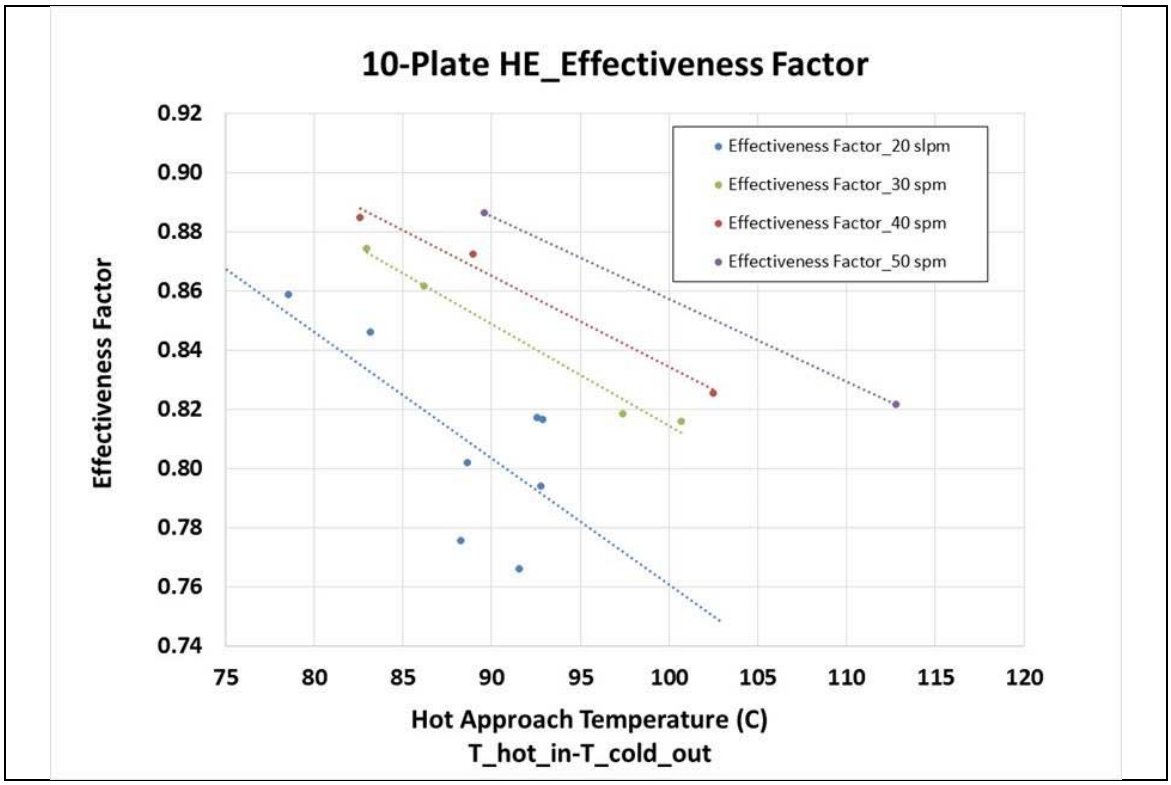

Figure 38 Calculated effectiveness of the ten-plate stack during the second test campaign.

In addition to the estimations made by CFD, based on the measured data, the measured heat transfer coefficients, HTC, for the tests at different flow rates were fit by a multivariable linear regression as a function of the cold air flow rate per plate, F_g, and the Log Mean Temperature Difference, LMTD, to extrapolate HTC at higher flow rates. The data fit the following equation:

HTC ($W/m^2/C$) = -13.6636+2.1555*F_g (slpm)+0.06231*LMTD (°C)

Using the equation above, the 10-plate stack would be expected to provide a 2.45 KW heat duty at a flow rate of 50 SLPM. This is approximately in agreement with the CFD results summarized in Table 10. Therefore, the multivariable regression analysis was used to estimate the number of heat exchanger plates required for a given thermal load. Table 12 shows the experimental results and those estimated by the multivariable regression equation. Although the heat duty performed by each plate should increase as the flow rate increases (until limited by pressure drop), the heat duty per plate was fixed to the value measured and the number of plates required to provide heat duty for the microturbine cases described in Table 2 and Table 3 were calculated. The results are shown in Table 12. Using the number of plates calculated, an approximate size of heat exchanger was also estimated. The heat exchanger was assumed to consist of separate modules of fifty plates each, arranged in rows and columns. Actual heat exchangers, or recuperators, for microturbines may be configured differently. For example, other work at Ceramatec has demonstrated the concept of making segmented, radial heat exchangers that wrap around turbine engines. Since the estimate is conservative, due to the assumption made on the value of heat duty per plate, the estimated size is likely the largest required to perform the desired heat duty.

Table 12
Performance Summary

	Lab	Extrapolated	C30	C65	C200
Air Flow (kg/s)	4.00E-05	4.00E-04	0.3051	0.5027	1.36
Air Flow (slpm)	5	50	35000	60000	160000
LMTD (°C)	275	125	100	100	100
HTC (W/m2-K)	14	102	118	136	136
# plates	10	10	600	900	2400
Heat Duty/ plate (W)	77	245	245	245	245
Total Heat Duty (kW)	0.77	2.45	147	221	588
Required Heat Duty (kW)			140	215	585
Approx. HX size, L x W x H, (m)	0.1 x 0.1 x 0.1	0.1 x 0.1 x 0.1	0.9 x 0.8 x 0.75	1.1 x 0.8 x 0.75	1.3 x 1.1 x 0.75

Project Summary

Analysis was used to determine microchannel and plate geometries for high effectiveness, compact, ceramic, microchannel heat exchangers that could provide the heat duty and effectiveness required for commercial microturbines. Low-cost methods of fabricating these heat exchangers were demonstrated. Heat exchangers were fabricated using these methods and tested. A stack of ten individual plates containing a series of microchannels was fabricated, connected to external flow manifolds, instrumented, and tested. The stack performed 2.45 kW of thermal duty and analysis showed that it could meet the goal of demonstrating 5-10 kW of thermal duty at an order of magnitude greater flow rates. Unfortunatley,these flow rates couldn't be produced in the laboratory. The analyses show that the stack was highly effective, operated at high temperatures, survived unplanned thermal transients, and would likely provide 5-10 kW heat duty at higher flow rates. Recommended future work would include confirming performance metrics at relevant flow rates and conditions, verifying reliability of stacks and connections during planned and unplanned transients, and performing long term test data.

c. Training and Professional Development

No activity.

d. How have the results been disseminated to communities of interest?

Results were presented at:

1. 16th International Symposium on Supercritical Carbon Dioxide Power Cycles, San Antonio, TX, March 29-31, 2016.
2. ASME Power and Energy Conference, Charlotte, NC, June 27- July 1, 2016.
3. Thermal Management 2016, Denver, CO, September 2-4, 2016.

e. Plans

Ceramatec has a roadmap to commercial development of ceramic, microcannel heat exchangers. Based on the positive results of this project, development will continue. Microturbine applications are targeted for market entry, although other applications are also being considered. In addition to market validation and cost verification, key technical milestones include:

Evaluation of thermal transient behavior
Verification of methods of joining ceramic components to metallic components
Verification of long term environmental stability and reliability.

Government assistance may be requested for demonstrating these technical milestones.

3. PRODUCTS:

What has the project produced?

A ten-plate heat exchanger and benchscale test apparatus.

4. PARTICIPANTS & OTHER COLLABORATING ORGANIZATIONS:

a. Participants (Ceramatec)

1. **Name:** Dr. Charles Lewinsohn
2. **Project Role:** Principal Investigator
3. **Nearest person month worked:** 3
4. **Contribution to Project:** Project Management, guidance on fabrication of heat exchanger plates, reporting.
5. **Funding Support:** NA
6. **Collaborated with individual in foreign country:** No
7. **Country(ies) of foreign collaborator:** NA
8. **Travelled to foreign country:** No
9. **If traveled to foreign country(ies), duration of stay:** 0 months

1. **Name:** Mr. Joseph Fellows
2. **Project Role:** Fabrication and Test Engineer
3. **Nearest person month worked:** 9
4. **Contribution to Project:** Development of process parameters, supervision of fabrication and testing.
5. **Funding Support:** NA
6. **Collaborated with individual in foreign country:** No
7. **Country(ies) of foreign collaborator:** NA
8. **Travelled to foreign country:** No
9. **If traveled to foreign country(ies), duration of stay:** 0 months

1. **Name:** Angela Anderson
2. **Project Role:** Lead Technician
3. **Nearest person month worked:** 36
4. **Contribution to Project:** Ms. Anderson processed material and operated equipment required to produce ceramic tape, lamination of heat exchanger plates, and high temperature densification of heat exchanger plates.
5. **Funding Support:** NA
6. **Collaborated with individual in foreign country:** No
7. **Country(ies) of foreign collaborator:** No
8. **Travelled to foreign country:** No
9. **If traveled to foreign country(ies), duration of stay:** 0 months

b. What other organizations have been involved as partners?

The Colorado School of Mines.

c. Have other collaborators or contacts been involved?
None.

6. CHANGES/PROBLEMS:

a. Changes in approach and reasons for change
None.

b. Actual or anticipated problems or delays and actions or plans to resolve them
No significant problems or delays.

c. Changes that have a significant impact on expenditures
None.

d. Significant changes in use or care of human subjects, vertebrate animals, and/or
Biohazards
None

e. Change of primary performance site location from that originally proposed
None.

7. SPECIAL REPORTING REQUIREMENTS: Mandatory
None.

8. BUDGETARY INFORMATION: Mandatory

	FY 15				FY 16			
	Q1	Q2	Q3	Q4	Q1	Q2	Q3	Q4
BASELINE								
Federal	$44,922	$44,923	$44,923	$44,923	$55,058	$55,058	$55,058	$55,057
Non-Federal	$11,237	$11,238	$11,237	$11,237	$13,763	$13,762	$13,763	$13,763
Total	$56,159	$56,161	$56,160	$56,160	$68,821	$68,820	$68,821	$68,820
ACTUAL								
Federal	$23,751	$63,784	$66,008	$86,315	$60,300	$61,889	$18,916	$18,959
Non-Federal	$0	$0	$71,359	$31,673	$0	$8,980	$0	$19,295
Total	$23,751	$63,784	$137,367	$117,988	$60,300	$70,869	$18,916	$38,254
VARIANCE								
Federal	$21,171	($18,861)	($21,085)	($41,392)	($5,242)	($6,831)	$36,142	$36,098
Non-Federal	$ 11,237	$11,238	($60,122)	($20,436)	$13,763	$4,782	$13,763	$(5,532)
Total	$32,408	($7,623)	($81,207)	($61,828)	$8,521	($2,049)	$49,905	$30,566